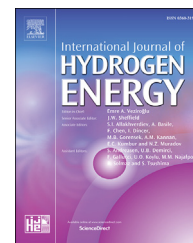




ELSEVIER

Available online at [www.sciencedirect.com](http://www.sciencedirect.com)

ScienceDirect

journal homepage: [www.elsevier.com/locate/hydro](http://www.elsevier.com/locate/hydro)

# Electrochemically active and robust cobalt doped copper phosphosulfide electro-catalysts for hydrogen evolution reaction in electrolytic and photoelectrochemical water splitting

Prasad Prakash Patel <sup>a</sup>, Oleg I. Velikokhatnyi <sup>b,c</sup>, Shrinath D. Ghadge <sup>a</sup>, Prashanth J. Hanumantha <sup>b</sup>, Moni Kanchan Datta <sup>b,c</sup>, Ramalinga Kuruba <sup>b</sup>, Bharat Gattu <sup>a</sup>, Pavithra Murugavel Shanthi <sup>a</sup>, Prashant N. Kumta <sup>a,b,c,d,e,\*</sup>

<sup>a</sup> Department of Chemical and Petroleum Engineering, Swanson School of Engineering, University of Pittsburgh, Pittsburgh, PA 15261, USA

<sup>b</sup> Department of Bioengineering, Swanson School of Engineering, University of Pittsburgh, Pittsburgh, PA 15261, USA

<sup>c</sup> Center for Complex Engineered Multifunctional Materials, University of Pittsburgh, PA 15261, USA

<sup>d</sup> Mechanical Engineering and Materials Science, Swanson School of Engineering, University of Pittsburgh, Pittsburgh, PA 15261, USA

<sup>e</sup> School of Dental Medicine, University of Pittsburgh, PA 15217, USA

## ARTICLE INFO

### Article history:

Received 15 December 2017

Received in revised form

21 February 2018

Accepted 22 February 2018

Available online 24 March 2018

### Keywords:

Hydrogen evolution reaction

Water splitting

Copper phosphide

Phosphosulfide

Sulfur doping

## ABSTRACT

The area of non-noble metals based electro-catalysts with electrochemical activity and stability similar or superior to that of noble metal electro-catalyst for efficient hydrogen production from electrolytic and photoelectrochemical (PEC) water splitting is a subject of intense research. In the current study, exploiting theoretical first principles study involving determination of hydrogen binding energy to the surface of the electro-catalyst, we have identified the  $(\text{Cu}_{0.83}\text{Co}_{0.17})_3\text{P}$ : x at. % S system displaying excellent electrochemical activity for hydrogen evolution reaction (HER). Accordingly, we have experimentally synthesized  $(\text{Cu}_{0.83}\text{Co}_{0.17})_3\text{P}$ : x at. % S (x = 10, 20, 30) demonstrating excellent electrochemical activity with an onset overpotential for HER similar to Pt/C in acidic, neutral as well as basic media. The highest electrochemical activity is exhibited by  $(\text{Cu}_{0.83}\text{Co}_{0.17})_3\text{P}$ :30 at. % S nanoparticles (NPs) displaying overpotential to reach  $100 \text{ mA cm}^{-2}$  in acidic, neutral and basic media similar to Pt/C. The  $(\text{Cu}_{0.83}\text{Co}_{0.17})_3\text{P}$ :30 at. % S NPs also display excellent electrochemical stability in acidic media for long term electrolytic and PEC water splitting process [using our previously reported  $(\text{Sn}_{0.95}\text{Nb}_{0.05})\text{O}_2$ : N-600 nanotubes (NTs) as the photoanode]. The applied bias photon-to-current efficiency obtained using  $(\text{Cu}_{0.83}\text{Co}_{0.17})_3\text{P}$ :30 at. % S NPs as the cathode electro-catalyst for HER in an H-type PEC water splitting cell (~4%) is similar to that obtained using Pt/C (~4.1%) attesting to the promise of this exciting non-noble metal containing system.

© 2018 Hydrogen Energy Publications LLC. Published by Elsevier Ltd. All rights reserved.

\* Corresponding author. Department of Bioengineering, 815C Benedum Hall, 3700 O'Hara Street, Pittsburgh, PA 15261, USA.

E-mail address: [pkumta@pitt.edu](mailto:pkumta@pitt.edu) (P.N. Kumta).

<https://doi.org/10.1016/j.ijhydene.2018.02.147>

0360-3199/© 2018 Hydrogen Energy Publications LLC. Published by Elsevier Ltd. All rights reserved.

## Introduction

Achieving sustainable, economic and clean energy supply by replacing hitherto technologies for energy production based on combustion of fossil fuels is one of the major energy related technological hurdles facing the globe today [1–6]. Incessant large dependence and consequent, vast consumption of fossil fuels has contributed to excessive emissions of greenhouse gases which has led to global climatic changes over the years placing significant stress on the environment [1–5]. Hence, at the risk of significantly compromising the environment, it is imperative to identify efficient, clean (low carbon footprint) and environmentally friendly energy sources that can be manufactured and produced in an economical fashion. This will enable the society to transition from an energy economy driven largely by fossil fuel based energy sources to non-carbonaceous fuels based economy with the aim of meeting the colossal global energy demand with minimum emission of greenhouse gases and thus, ensuring a sustainable society driven by environmental recyclable resources of solar, wind, and water [1,4,7–12]. Along these lines, hydrogen has been identified as the primary potential energy source due to its low carbon footprint, high energy density (120 MJ/kg for H<sub>2</sub> higher than 44.4 MJ/kg for Gasoline) and the ability to offer clean, reliable and affordable energy supply for meeting the tremendous global energy demand [13]. In addition, hydrogen is an important chemical with a global production rate of 50 billion kg per year that is mainly used in petroleum refining and production of ammonia based fertilizers as well as other important industrial chemicals [14].

Current approaches for H<sub>2</sub> production mainly involve steam reforming of natural gas, coal gasification and the partial oxidation of hydrocarbons [15,16]. The drawbacks of these processes are high operating temperature and emission of CO<sub>2</sub>, the undesired greenhouse gas pollutant [15,16]. With the increase in global demand of H<sub>2</sub> on the grounds of its important applications mentioned above, processing of vast amount of fossil fuels is not viable. Hence, it is of utmost importance to produce hydrogen from non-carbonaceous and environmentally friendly tools with minimum emission of greenhouse gases.

Electricity driven water splitting (water electrolysis coupled to renewable energy source such as solar, wind, etc.) and photoelectrochemical (PEC) water splitting (where electricity is generated from suitable semiconductor material used as the photoanode and then used in tandem to drive the HER to produce H<sub>2</sub> at the cathode) are promising approaches, as they involve production of hydrogen from non-carbonaceous sources with no emission of greenhouse gases whatsoever and no toxic byproducts [17,18]. In these processes, electricity is used for driving the water splitting reaction ( $\Delta G^\circ = 237.13 \text{ kJ mol}^{-1}$  or 1.23 eV) [19]. However, one of the factors limiting the commercial development of electrolytic water splitting process is the high capital cost, mainly due to the use of expensive precious noble metal electro-catalysts (e.g. Pt, IrO<sub>2</sub>) that albeit exhibit excellent electrochemical activity with minimum overpotential and long term electrochemical stability. The development of PEC water splitting systems is however, constrained by insufficient solar-to-

hydrogen (STH) efficiency and limited long term stability. Moreover, the use of noble metal electro-catalysts (Pt, Pd) could be a concern for future applications in PEC systems.

The development of novel non-noble metals based electro-catalyst exhibiting similar/superior electrochemical activity with minimum overpotential and stability than state of the art electro-catalyst (Pt/C) for hydrogen evolution reaction (HER), which constitutes half of the water splitting reaction, will be a significant breakthrough in reduction of capital cost of water splitting cells. In addition to proton exchange membrane (PEM) based water electrolysis and PEC water splitting involving operation in acidic media (pH=0), HER is also very important in the microbial electrolysis cell (MEC) which involves production of hydrogen from wastewater (neutral media, pH=7) through microbes assisted degradation of organic waste and electrolytic water splitting for generation of hydrogen in basic media (pH=14) [20]. An ideal non-noble metals based HER electro-catalyst should exhibit superior electrochemical active surface area, high electronic conductivity, superior charge transfer kinetics, high current density at low overpotential, excellent electrochemical activity for HER and superior long term electrochemical stability for continuous H<sub>2</sub> production over long period of operation in acidic, neutral as well as basic media.

In the pursuit of identification and development of cheap, highly electrochemically active and stable electro-catalysts for HER, there have been many pioneering studies reported on non-noble metals based nitride and sulfide based electro-catalysts exhibiting promising performance for HER such as MoS<sub>2</sub> [21,22], CoSe<sub>2</sub> [23], Co<sub>0.6</sub>Mo<sub>1.4</sub>N<sub>2</sub> [24], MoSe<sub>2</sub> [25], NiMoN<sub>x</sub> [26], WS<sub>2</sub> [27], etc. Earth-abundant transition metal phosphides (TMPs) are also important materials exhibiting good electronic conductivity and are widely utilized as catalysts in hydrodesulfurization (HDS), hydrodenitrogenation as well as anode materials for Li ion batteries [28–32]. Both HDS and HER rely on reversible binding of hydrogen on the catalyst surface. In HDS, hydrogen dissociates on the catalyst surface and reacts with sulfur forming H<sub>2</sub>S which creates a reactive sulfur vacancy site [14], while in HER, the protons bind to the electro-catalyst surface promoting HER and accordingly generating H<sub>2</sub> gas [28]. Thus, TMPs are also considered as active electro-catalysts for HER. On the basis of these developments, there has correspondingly been significant research efforts directed to the study of TMPs as electro-catalysts for HER such as Ni<sub>2</sub>P [33,34], CoP [20,28,35,36], MoP [37], FeP [32,38], WP [39], WP<sub>2</sub> [40], etc., wherein, these electro-catalysts have shown noticeable electrochemical activity for HER.

With the principle aim of this study targeted at the design and development of cheap non-noble metals based electro-catalysts displaying similar/superior electrochemical activity for HER and stability than that of Pt/C, in this report we describe copper phosphide (Cu<sub>3</sub>P) based electro-catalyst system that has been studied as a potential electro-catalyst for HER, on the grounds of promising HER performance displayed by self-supported Cu<sub>3</sub>P nanowire arrays [41]. In the present study, therefore, theoretical first-principles electronic structure calculations involving determination of the hydrogen binding energy ( $\Delta G_{\text{H}^*}$ ) to the surface of specific electro-catalysts, has been carried out to identify and develop

suitable  $\text{Cu}_3\text{P}$  based electro-catalyst systems exhibiting excellent electrochemical activity for HER similar to that of noble metal electro-catalyst system (Pt). Based on the theoretical calculations, cobalt doped copper phosphosulfide denoted as  $(\text{Cu}_{0.83}\text{Co}_{0.17})_3\text{P}$ : x at. % S (x = 10, 20, 30) of different compositions have been explored as a suitable electro-catalyst system for HER, for the very first time and presented in this report to the best of our knowledge. Cobalt is selected as the preferred dopant for  $\text{Cu}_3\text{P}$  on the grounds of its ability to offer promotional effect in  $\text{MoS}_2$  as reported earlier [42,43]. Thus, the incorporation of cobalt in  $\text{Cu}_3\text{P}$  is expected to offer increased number of catalytically active sites (due to a decrease in  $\Delta G_{\text{H}^*}$ ) resulting in improved catalytic activity (lower polarization losses) for HER, which is verified by the theoretical first-principles electronic structure calculations reported in this study [42–46]. The rationale for selection of sulfur is that the most active sites for TMPs in HDS reaction are considered to be phosphosulfide formed during the reaction and thus, sulfur is known to play an important role in improving the catalytic activity of metal phosphides for HDS [31,47,48]. Hence, sulfur is incorporated in  $\text{Cu}_3\text{P}$  to achieve electronic and molecular states similar to that seen during HDS operating conditions and thus, achieve excellent electrochemical activity for HER. In addition, incorporation of S into the  $\text{Cu}_3\text{P}$  lattice will offer improved electronic conductivity which will potentially also enable fast charge transfer kinetics. Thus, the simultaneous incorporation of Co and S into the  $\text{Cu}_3\text{P}$  lattice offers unique opportunity for tailoring the electronic structure, physical, electronic and electro-catalytic properties of  $\text{Cu}_3\text{P}$  to match the noble metal electro-catalyst systems. As a result, the  $(\text{Cu}_{0.83}\text{Co}_{0.17})_3\text{P}$ : x at. % S (x = 10, 20, and 30) has been explored for the first time in this report, to the best of our knowledge as the universal electro-catalyst system for HER in electrolytic water splitting encompassing all three acidic, neutral and basic media in this study.

In addition,  $(\text{Cu}_{0.83}\text{Co}_{0.17})_3\text{P}$ :S is also studied as HER electro-catalyst in PEC water splitting cell using  $(\text{Sn}_{0.95}\text{Nb}_{0.05})\text{O}_2$ :N-600 nanotubes (NTs) as the photoanode [8]. The photoelectrochemical characterization has been carried out in an H-type cell, in which the cathode (where HER occurs) and photoanode (where water oxidation reaction takes place) are separated by the Nafion 115 membrane (DuPont) [8]. As reported earlier by us [8], the maximum applied bias photon-to-current efficiency (ABPE) of ~4.1% was obtained using  $(\text{Sn}_{0.95}\text{Nb}_{0.05})\text{O}_2$ :N-600 NTs as the photoanode and Pt (wire) as cathode at an applied potential of -0.75 V (vs RHE), which is the highest ABPE obtained so far compared to other semiconductor materials studied as photoanode for PEC water splitting such as  $\text{TiO}_2$ ,  $\text{ZnO}$  and  $\text{Fe}_2\text{O}_3$  [8,10,49–52]. However, with the goal of completely replacing Pt with novel non-noble metals based electro-catalyst exhibiting excellent electrochemical activity for HER and stability similar/superior than that of Pt/C, the  $(\text{Cu}_{0.83}\text{Co}_{0.17})_3\text{P}$ :S system is also studied herein as the HER electro-catalyst to achieve similar/superior ABPE than that of Pt/C. This combined approach will help in progressing towards non-noble metals based electro-catalysis which will result in significant reduction in the capital cost of electrolytic and PEC water splitting system and thus, likely aid in their commercial development for efficient and economic production of hydrogen in environmentally friendly

manner. This is indeed a very relevant and represents an important part of today's intense research activity which will offer massive environmental, economic and technological benefits in the short as well as long term.

Thus, the present report documents for the first time the theoretical and experimental studies focused on detailing the electrochemical performance of nanostructured cobalt doped copper phosphosulfide system, i.e.,  $(\text{Cu}_{0.83}\text{Co}_{0.17})_3\text{P}$ : x at. % S (x = 10, 20, 30) of different compositions serving as cathode electro-catalysts for HER in electrolytic and photoelectrochemical water splitting [using our previously reported  $(\text{Sn}_{0.95}\text{Nb}_{0.05})\text{O}_2$ :N-600 NTs as the photoanode], synthesized using a simple synthesis route at low temperature of 250 °C.

## Computational methodology and details

The electro-catalytic activity of an electro-catalyst can be described by a parameter,  $\Delta G_{\text{H}^*}$  which is the free energy of adsorbed hydrogen atom on the electro-catalyst surface.  $\Delta G_{\text{H}^*}$  is desired to be close to 0 eV, which indicates the ease of adsorption and desorption of hydrogen atoms from the electro-catalyst surface [53–55].  $\Delta G_{\text{H}^*}$  is represented by the following relation:  $\Delta G_{\text{H}^*} = \Delta E_{\text{H}^*} + \Delta \text{ZPE} - T\Delta S$ . The reaction energy  $\Delta E_{\text{H}^*}$  is calculated using the density functional theory methodology (DFT) as following:

$$\Delta E_{\text{H}^*} = E(\text{Mat} + n\text{H}) - E(\text{Mat} + (n-1)\text{H}) - 1/2 E(\text{H}_2),$$

where  $E(\text{Me} + n\text{H})$  is the total energy of a metal surface slab with the n hydrogen atoms adsorbed on the surface,  $E(\text{Me} + (n-1)\text{H})$  is the total energy of the corresponding metal surface slab with (n-1) hydrogen atoms (after removal of one hydrogen atom from the given site) and  $E(\text{H}_2)$  is the total energy of the hydrogen molecule in the gas phase.

$\text{Cu}_3\text{P}$  has a hexagonal crystal structure  $\text{P6}_3\text{cm}$  (group# 185) with 24 atoms in the unit cell with the following lattice parameters:  $a = b = 6.959 \text{ \AA}$  and  $c = 7.143 \text{ \AA}$  [56]. For estimation of  $\Delta E_{\text{H}^*}$ , the crystallographic surface (0001) has been chosen with the active sites located above Cu 4b-type of the lattice sites as shown in Fig. 1a. Co and S atoms are also shown in this figure. In all the calculations, 1 monolayer of H-coverage of the (0001) surface has been considered. Also, the zero point energy correction  $\Delta \text{ZPE}$  minus the entropy term  $T\Delta S$  has been taken equal to 0.24 eV, as it was used by Nørskov et al. [55], for calculations of  $\Delta G_{\text{H}^*}$  for all materials considered in that study.

All the surface slabs consist of five copper and two phosphorus layers with fixed three lower copper and one phosphorus layers with the lattice parameters corresponding to the calculated bulk crystal structures. The remaining three top layers were allowed to relax together with all the adsorbed hydrogen atoms on the surface. The slab was separated from its image by a vacuum layer of ~20 Å. Since, the purpose of the present theoretical study is to bring to light the effects of Co and S elements on the overall catalytic activity of  $\text{Cu}_3\text{P}$ , only one composition of each dopant has been chosen for the calculation of  $\Delta G_{\text{H}^*}$  and other properties of the corresponding compounds. Thus, accordingly, the free energies of hydrogen adsorption to the surface have been calculated for pure  $\text{Cu}_3\text{P}$ ,  $(\text{Co}_{0.17}\text{Cu}_{0.83})_3\text{P}$  and  $(\text{Co}_{0.17}\text{Cu}_{0.83})_3\text{P}_{0.5}\text{S}_{0.5}$  compositions. These

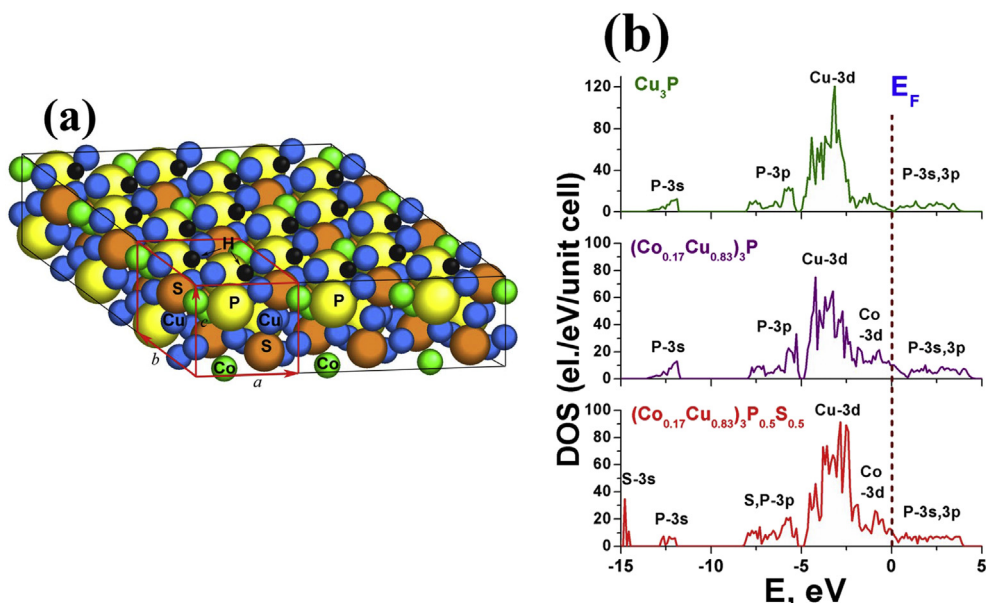


**Fig. 1** – (a) Surface slab of  $\text{Cu}_3\text{P}$  structure doped with Co and S. Red box is the unit cell used in all DFT calculations. Small blue balls – Cu, small green – Co, large yellow – P, large orange – S, the smallest black – hydrogen atoms attached to the surface on active sites. Vectors  $a$ ,  $b$ , and  $c$  correspond to the bulk crystal structure lattice parameters, (b) Calculated total density of electronic states for pure  $\text{Cu}_3\text{P}$ ,  $(\text{Co}_{0.17}\text{Cu}_{0.83})_3\text{P}$ , and  $(\text{Co}_{0.17}\text{Cu}_{0.83})_3\text{P}_{0.5}\text{S}_{0.5}$ ; Fermi level is set to zero energy. Labels indicate major contributions from corresponding projected electronic states. (For interpretation of the references to color in this figure legend, the reader is referred to the Web version of this article.)

compositions have been chosen from the crystallographic consideration of the  $\text{Cu}_3\text{P}$  elementary unit cell.

In the present study for all the DFT calculations, the Vienna Ab-initio Simulation Package (VASP) has been used within the projector-augmented wave [57] method [58–60] and the generalized gradient approximation for the exchange-correlation energy functional in a form suggested by Perdew and Wang [61]. This program calculates the electronic structure and via the Hellmann-Feynman theorem, the interatomic forces are determined from first-principles. The standard PAW potentials were employed for the Cu, Co, P, and S potentials containing eleven, nine, five, and six valence electrons, respectively.

For all the materials considered in this study, the plane wave cutoff energy of 520 eV has been chosen to maintain a high accuracy of the total energy calculations. The lattice parameters and internal positions of atoms were fully optimized employing the double relaxation procedure and consequently, the minima of the total energies with respect to the lattice parameters and internal ionic positions have been determined. This geometry optimization was obtained by minimizing the Hellman-Feynman forces via a conjugate gradient method, so that the net forces applied on every ion in the lattice are close to zero. The total electronic energies were converged to within  $10^{-5}$  eV/un cell resulting in the residual force components on each atom to be lower than 0.01 eV/Å/atom thus, allowing for an accurate determination of the internal structural parameters for the material. The Monkhorst-Pack scheme was used to sample the Brillouin Zone (BZ) and generate the  $\mathbf{k}$ -point grid for all the materials considered in the present study.

## Results and discussion

### Theoretical study illuminating the effect of Co and S on the electrochemical activity and structural stability of the selected $(\text{Cu},\text{Co})_3\text{P}:\text{S}$ compounds

The electro-catalytic activity of virtually any electro-catalyst is expected to depend on the electronic structure as well as the electronic conductivity, while the long term stability of the electro-catalyst is assumed to qualitatively depend on the cohesive energy of the system. The effect of compositions on the electronic and catalytic properties as well as the compositional effects on the structural stability of the material could be understood from the theoretical considerations.

As mentioned in earlier section of the manuscript, the main purpose of the computational component of the present study is to explore the effects of Co and S dopants on the electro-catalytic activity as well as the structural and chemical stability of  $\text{Cu}_3\text{P}$  during HER. For these purposes the electronic structure, hydrogen adsorption free energies  $\Delta G_{\text{H}^*}$  as well as the cohesive energies have been considered as a qualitative measure of the structural and chemical stability, and they have all been calculated for the different materials considered in the current study.

It should be noted that for a good HER electro-catalyst, it is essential that the free energy of adsorbed H ( $\Delta G_{\text{H}^*}$ ) should be close to 0 such that the hydrogen atoms would be able to easily adsorb and desorb from the surface during HER. Thus, the task of identifying a good electro-catalyst material for HER could partially be reduced to estimation of the free binding energy of

**Table 1 – Calculated free energy of hydrogen adsorption  $\Delta G_{H^+}$ , the electronic density of states at the Fermi level, and cohesive energy  $-E_{coh}$  for all materials considered in the present study.**

Materials	$\Delta G_{H^+}$ (in eV)	$N(E_F)$ el./eV/ unit cell	$-E_{coh}$ (in eV/f.unit)
Cu <sub>3</sub> P	0.31	1.5	13.96
(Co <sub>0.17</sub> Cu <sub>0.83</sub> ) <sub>3</sub> P	0.16	10.1	14.94
(Co <sub>0.17</sub> Cu <sub>0.83</sub> ) <sub>3</sub> P <sub>0.5</sub> S <sub>0.5</sub>	0.10	11.7	14.48

the hydrogen to the electro-catalytic surface. Modification of the electro-catalytic surface electronic structure by changing the chemical composition in such a way that the resulting  $\Delta G_{H^+}$  becomes close to zero, may also substantially improve the electro-catalytic activity of the material. For these purposes therefore, the hydrogen binding free energy ( $\Delta G_{H^+}$ ) has been obtained from DFT calculations by subtracting the free energy of the pristine electro-catalyst surface and a half of a hydrogen molecule in the gas phase from the corresponding free energy of the electro-catalyst surface with hydrogen atom bonded to the site. The methodology is very similar to that presented by Nørskov et al. in previous report [55].

Table 1 shows a tabulation of the free energies  $\Delta G_{H^+}$ , density of states at the Fermi level, and cohesive energies for all the different materials considered in the present study. It can be seen that the hydrogen adsorption to the surface of pure Cu<sub>3</sub>P is too weak and quite far from the optimal value resulting in an inferior expected electro-catalytic activity for HER. It may be explained from the electronic structure consideration that since Cu-3d electrons locate relatively deep below the Fermi level the hybridization between these electrons and H-1s states located above the Fermi level becomes very weak thus, making adsorption of hydrogen atoms practically impossible (Fig. 1b).

An introduction of Co into the Cu<sub>3</sub>P lattice substituting for Cu decreases  $\Delta G_{H^+}$  noticeably bringing its value toward the more optimal energy value. In this case, new Co-3d electronic states are created locating in the vicinity of the Fermi level and hybridize with H-1s electrons more strongly resulting in stronger interaction between hydrogen atoms and the material's surface. Such a modification of the electronic structure is expected to improve the electro-catalytic activity of the electro-catalyst (Fig. 1b). Further substitution of phosphorus for sulfur in (Cu,Co)<sub>3</sub>P results in the hydrogen adsorption energy being even more close to the zero value of  $-0.1$  eV. This indicates a further increase in the strength of the hydrogen-surface interaction due to the stronger H–S bonds compared to the H–P bonds (bond dissociation energies for diatomic molecules are  $353.6 \text{ kJ mol}^{-1}$  vs.  $297.0 \text{ kJ mol}^{-1}$  respectively [62]. This effect of the sulfur addition is expected to noticeably further improve the electro-catalytic activity of (Cu,Co)<sub>3</sub>P:S compound. Thus, using the concept of the free energy of the hydrogen adsorption to the electro-catalytic surface, the present study has shown positive effect of introduction of Co and S on the expected catalytic activity of Cu<sub>3</sub>P electrocatalyst for HER.

Another goal of the present study as outlined earlier is to investigate the effect of Co and S doping on the electronic conductivity of Cu<sub>3</sub>P. Since, in general the metallic conductivity is proportional to the density of states at the Fermi level

$N(E_F)$ , it provides an opportunity to qualitatively estimate the influence of those dopants on the overall electronic conductivity of Cu<sub>3</sub>P. The electronic structure of Cu<sub>3</sub>P calculated in the present study demonstrates slight metal-type conductivity with non-zero density of the electronic states at the Fermi level (Fig. 1b) which is opposite to the experimental data indicating this material is a semiconductor with a narrow band gap  $\sim 0.8$  eV between the valence and conduction electronic zones [63]. This discrepancy with experimental data attributes to the inherent inability of the DFT methodology to reproduce correctly the band gaps of insulators and semiconductors with the well-known tendency of DFT to underestimate the corresponding band gap energy values on average by 30–50%. Also, some materials with narrow band gaps may very well be presented as metal-type conductors. Nevertheless, in the case of Cu<sub>3</sub>P, the value of  $N(E_F)$  is very small indicating poor electronic conductivity of the compound. The introduction of Co into the system however, changes the electronic structure in such a way that the presence of Co-3d electrons in the vicinity of the Fermi level increases the number of electrons and thus, improves the overall electronic conductivity of the material (Fig. 1b). An additional introduction of S into the (Cu,Co)<sub>3</sub>P lattice by substituting for P atoms further improves the conductivity (Fig. 1b), since sulfur atoms bind to lower number of Cu valence electrons than phosphorus atoms (2 instead of 3 electrons for each S atom) rendering some of Cu valence electrons readily available in the system and thus increasing the number of total charge carriers at the Fermi level, as indicated in Table 1. Such an increase in the electronic conductivity also positively contributes to the overall electro-catalytic activity of the material along with hydrogen adsorption energy to the surface of the doped material.

The last aspect to be highlighted in the present theoretical study is the structural and electrochemical stability of the system for which the cohesive energy  $E_{coh}$  can be considered as a qualitative indicator. The higher the  $E_{coh}$  (the more negative value), the more durable is the electro-catalyst material and thus, can be expected to display long term stability and durability when considered over the entire duration of the long term HER electro-catalytic process.  $E_{coh}$  calculated for all the materials are collected in Table 1. It can be again seen that an introduction of Co into the Cu<sub>3</sub>P lattice substantially improves the overall stability of (Co<sub>0.17</sub>Cu<sub>0.83</sub>)<sub>3</sub>P due to the presence of much stronger Co–P bonds in comparison to Cu–P [calculated  $E_{coh}$  for pure Cu<sub>3</sub>P is  $-13.96$  eV/f.un. vs.  $-14.94$  eV/f.un. for (Co<sub>0.17</sub>Cu<sub>0.83</sub>)<sub>3</sub>P]. However, further introduction of S into the (Co<sub>0.17</sub>Cu<sub>0.83</sub>)<sub>3</sub>P compound results in relative lowering of the cohesive energy that occurs mainly due to the lower ionic charge of S<sup>2-</sup> vs. P<sup>3-</sup> and thus, leads to significantly weakening the electrostatic component of Cu–S and Co–S bonds than those of Cu–P and Co–P ionic bonds. Nevertheless, even the relatively less stable (Co<sub>0.17</sub>Cu<sub>0.83</sub>)<sub>3</sub>P<sub>0.5</sub>S<sub>0.5</sub> compound is more stable than pure Cu<sub>3</sub>P, which makes this material likely more stable and capable of withstanding the harsh electrochemical conditions during HER as validated by the experimental results discussed in the sections to follow.

Thus, based on the results of the DFT study, (Cu,Co)<sub>3</sub>P:S is expected to demonstrate improved electro-catalytic activity due to quite optimal hydrogen adsorption energy and high

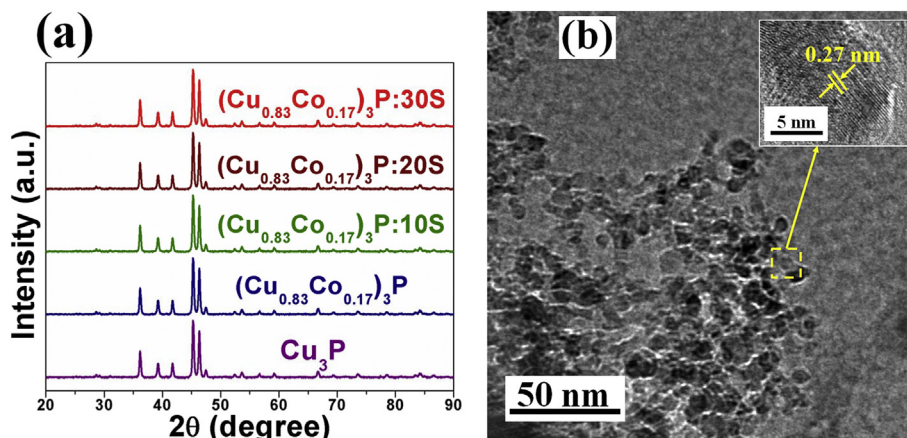


**Fig. 2** – (a) The XRD patterns of pure  $\text{Cu}_3\text{P}$  nanoparticles (NPs),  $(\text{Cu}_{0.83}\text{Co}_{0.17})_3\text{P}$  NPs and  $(\text{Cu}_{0.83}\text{Co}_{0.17})_3\text{P}:\text{S}$  NPs of different S concentration in wide angle  $2\theta$  scan, (b) The bright field TEM image of  $(\text{Cu}_{0.83}\text{Co}_{0.17})_3\text{P}:\text{S}$  NPs, (c) SEM micrograph with EDX spectrum of  $(\text{Cu}_{0.83}\text{Co}_{0.17})_3\text{P}:\text{S}$  NPs, (d) Elemental x-ray maps of  $(\text{Cu}_{0.83}\text{Co}_{0.17})_3\text{P}:\text{S}$  NPs.

electronic conductivity together with good structural and chemical stability which altogether make this material a likely good candidate for demonstrating structural stability and high electro-catalytic performance response suitable for HER. The theoretical results presented here are accordingly experimentally verified by synthesizing and characterizing different compositions of  $(\text{Cu}_{0.83}\text{Co}_{0.17})_3\text{P}:\text{x}$  at. % S ( $x = 10, 20, 30$ ) corresponding to different S concentrations to systematically study and illustrate the effect of different S concentrations on the electrochemical properties of  $(\text{Cu}_{0.83}\text{Co}_{0.17})_3\text{P}:\text{S}$  that are further discussed in the following sections of the manuscript.

#### Synthesis and characterization of theoretically predicted $(\text{Cu}_{0.83}\text{Co}_{0.17})_3\text{P}$ nanoparticles (NPs) and $(\text{Cu}_{0.83}\text{Co}_{0.17})_3\text{P}:\text{x}$ at. % S NPs ( $x = 10, 20, 30$ ) compositions for HER

##### Structural characterization of $\text{Cu}_3\text{P}$ , $(\text{Cu}_{0.83}\text{Co}_{0.17})_3\text{P}$ and $(\text{Cu}_{0.83}\text{Co}_{0.17})_3\text{P}:\text{x}$ at. % S NPs ( $x = 10, 20, 30$ )

The XRD pattern of the pure  $\text{Cu}_3\text{P}$  NPs (Fig. 2a) synthesized by heat treatment of  $\text{CuCl}_2 \cdot 2\text{H}_2\text{O}$  and  $\text{NaH}_2\text{PO}_4 \cdot \text{xH}_2\text{O}$  in UHP-argon atmosphere at  $250^\circ\text{C}$  and subsequent water-wash shows a hexagonal structure (JCPDS card no: 71-2261) with lattice parameters,  $a = b = 0.6959$  nm,  $c = 0.7413$  nm and a molar volume ( $V_m$ )  $\sim 31.2$  cm<sup>3</sup> mol<sup>-1</sup>, which is in good agreement with the literature value [64]. The XRD patterns of  $(\text{Cu}_{0.83}\text{Co}_{0.17})_3\text{P}$  NPs and  $(\text{Cu}_{0.83}\text{Co}_{0.17})_3\text{P}:\text{S}$  NPs of different S concentration, shown in Fig. 2a, show peaks corresponding to single phase hexagonal structure similar to that of  $\text{Cu}_3\text{P}$  without any other peaks of undesired secondary phase. This suggests incorporation of Co and S in lattice of  $\text{Cu}_3\text{P}$  for  $(\text{Cu}_{0.83}\text{Co}_{0.17})_3\text{P}:\text{S}$  NPs of different composition. The lattice parameters and molar volume of  $(\text{Cu}_{0.83}\text{Co}_{0.17})_3\text{P}$  NPs and  $(\text{Cu}_{0.83}\text{Co}_{0.17})_3\text{P}:\text{S}$  NPs of different S concentration (calculated using the least square refinement technique) are given in Table 2.

The lattice parameters and molar volume of  $(\text{Cu}_{0.83}\text{Co}_{0.17})_3\text{P}$  NPs are slightly lower than that of pure  $\text{Cu}_3\text{P}$  NPs which can be due to the smaller ionic radius of cobalt ion than that of copper ion [65]. However, there is a slight increase in the

lattice parameters and molar volume of  $(\text{Cu}_{0.83}\text{Co}_{0.17})_3\text{P}:\text{S}$  NPs in comparison to pure  $\text{Cu}_3\text{P}$  NPs and  $(\text{Cu}_{0.83}\text{Co}_{0.17})_3\text{P}$  NPs. The lattice parameters and molar volume of  $(\text{Cu}_{0.83}\text{Co}_{0.17})_3\text{P}:\text{S}$  NPs increase slightly with increase in S concentrations indicating the slight lattice expansion upon incorporation of S which is similar to earlier reports [66,67]. The TEM bright field image of the representative composition of  $(\text{Cu}_{0.83}\text{Co}_{0.17})_3\text{P}:\text{S}$  NPs, shown in Fig. 2b, shows that the nanoparticles are in the range of  $\sim 7$ – $10$  nm. The HRTEM image (Fig. 2b) shows lattice fringes with a spacing of  $\sim 0.27$  nm which corresponds well with the (112) inter-planer spacing of  $\text{Cu}_3\text{P}$  and indicates lattice expansion which is in agreement with the XRD analyses which is similar to earlier reports [66–68]. The SEM image along with the EDX pattern of the same representative composition  $(\text{Cu}_{0.83}\text{Co}_{0.17})_3\text{P}:\text{S}$  NPs, is shown in Fig. 2c. The EDX pattern confirms the presence of Cu, Co, S and P in  $(\text{Cu}_{0.83}\text{Co}_{0.17})_3\text{P}:\text{S}$  NPs (Fig. 2c). The quantitative elemental composition analysis (from EDX) of  $(\text{Cu}_{0.83}\text{Co}_{0.17})_3\text{P}:\text{S}$  NPs shows the measured elemental composition of Cu, Co, S and P to be close to the nominal composition (Fig. 2c). Elemental x-ray maps of Cu, Co, S and P, shown in Fig. 2d, indicates a homogeneous distribution of elements in the representative composition of  $(\text{Cu}_{0.83}\text{Co}_{0.17})_3\text{P}:\text{S}$  NPs with no evidence of any segregation at any specific site.

Chemical oxidation states of Cu, Co, S and P were also studied using x-ray photoelectron spectroscopy (XPS) analysis performed on NPs of pure  $\text{Cu}_3\text{P}$  and  $(\text{Cu}_{0.83}\text{Co}_{0.17})_3\text{P}:\text{S}$  NPs, respectively. The XPS spectrum in the Cu  $2p_{3/2}$  region for pure  $\text{Cu}_3\text{P}$  NPs shows a peak  $\sim 932.9$  eV (Fig. 3a), which is similar to earlier report [41]. The XPS spectrum in the P  $2p$  region for pure  $\text{Cu}_3\text{P}$  NPs, shown in Fig. 3b, shows two peaks at  $\sim 129.5$  eV and  $\sim 133.8$  eV. The peak at  $\sim 932.9$  eV in the Cu  $2p_{3/2}$  region and the peak at  $\sim 129.5$  eV correspond to binding energies of Cu and P in pure  $\text{Cu}_3\text{P}$  NPs [41,69]. The peak at  $\sim 133.8$  eV in the P  $2p$  region corresponds to oxidation of P related to presence of  $(\text{PO}_4^{3-})$  forming possibly owing to air exposure during handling of pure  $\text{Cu}_3\text{P}$  NPs (Fig. 3b) [14]. It is noteworthy to note that the peak at  $\sim 932.9$  eV in the Cu  $2p_{3/2}$  region of pure  $\text{Cu}_3\text{P}$  NPs reflects higher binding energies than that of metallic Cu

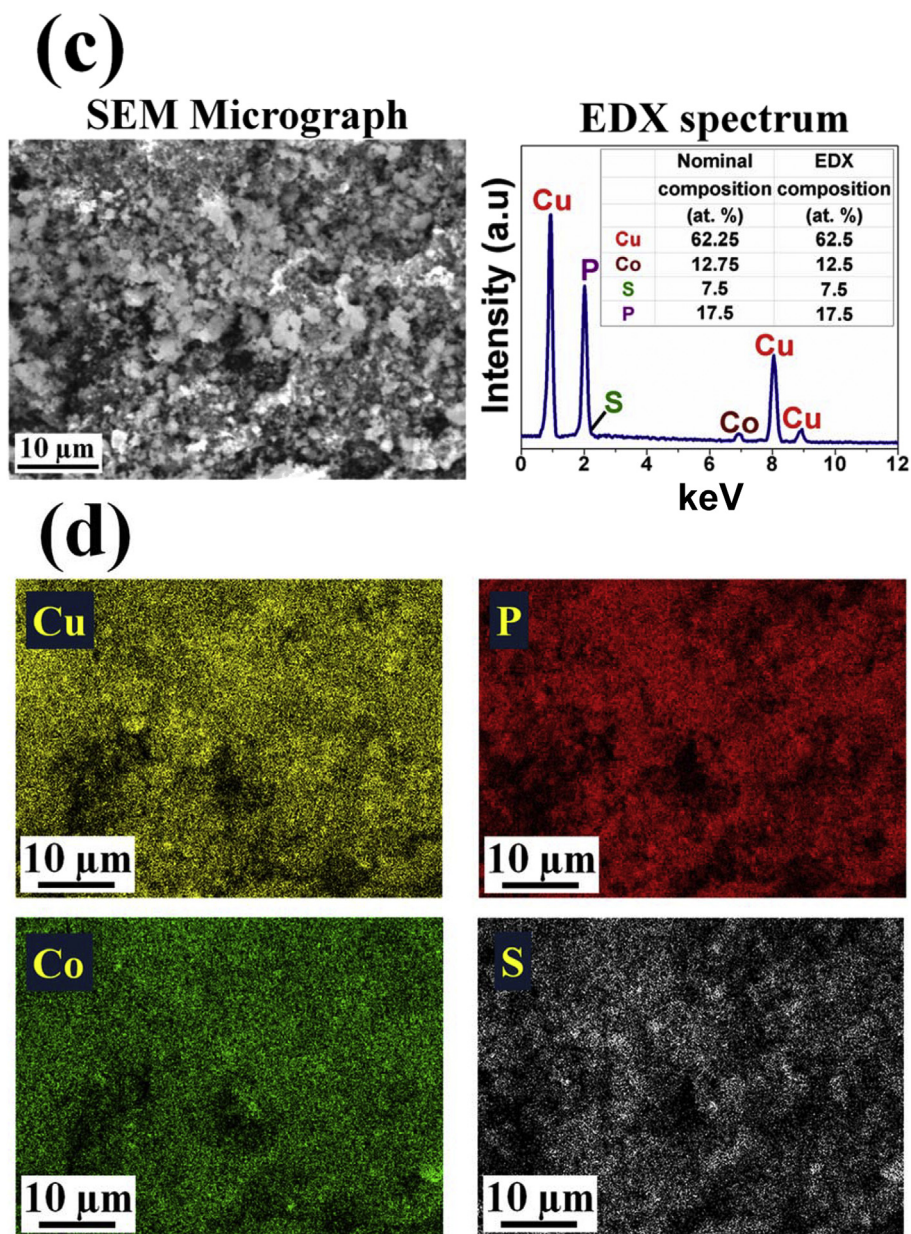


Fig. 2 – (continued).

(~932.6 eV) [70] and the peak at ~129.5 eV in P 2p region of pure  $\text{Cu}_3\text{P}$  NPs is at a lower binding energies than that of elemental P (~130.2 eV) [69], respectively. This indicates presence of Cu (metal centers) with positive partial charge ( $\delta^+$ ) and P (pendant bases) with negative partial charge ( $\delta^-$ ) close to metal center and thus, suggesting transfer of electrons from Cu to P and modification of the charge density of Cu and P in pure  $\text{Cu}_3\text{P}$  NPs [20]. There is also a positive shift of ~0.5 eV seen in peak in the Cu 2p<sub>3/2</sub> region for  $(\text{Cu}_{0.83}\text{Co}_{0.17})_3\text{P}:3\text{OS}$  NPs, which can possibly be due to transfer of electrons from Cu to S and correspondingly, modification of the charge density of phosphosulfide (Fig. 3a) [67]. The XPS spectrum of  $(\text{Cu}_{0.83}\text{Co}_{0.17})_3\text{P}:3\text{OS}$  NPs in the P 2p region shows only one peak at ~129.5 eV corresponding to P in  $\text{Cu}_3\text{P}$  [69] or CoP [71] (Fig. 3b). However, the peak corresponding to oxidized P (at ~133.8 eV

which is seen for pure  $\text{Cu}_3\text{P}$  as discussed earlier) arising due to air exposure of the phosphide material during handling is absent for  $(\text{Cu}_{0.83}\text{Co}_{0.17})_3\text{P}:3\text{OS}$  NPs (Fig. 3b) which can be due to likely stabilization of phosphide towards oxidation following the incorporation of S in the phosphide (as also seen earlier [14,71]). The exact reason is unknown at present warranting further study.

The XPS spectrum in the Co 2p<sub>3/2</sub> region for  $(\text{Cu}_{0.83}\text{Co}_{0.17})_3\text{P}:3\text{OS}$  NPs, shown in Fig. 3c, shows a peak at ~779.5 eV (which corresponds to Co in CoP [28]) is shifted by ~0.3 eV to higher binding energy than that of the typical peak (at ~779.2 eV) in the Co 2p<sub>3/2</sub> region of CoP [28], which can be due to transfer of electrons from Co to S [67]. The peak at ~779.5 eV in Co 2p<sub>3/2</sub> region of  $(\text{Cu}_{0.83}\text{Co}_{0.17})_3\text{P}:3\text{OS}$  NPs (Fig. 3c) is also at higher binding energies than that of metallic Co

**Table 2 – Results of structural and electrochemical characterization for HER of pure Cu<sub>3</sub>P NPs, (Cu<sub>0.83</sub>Co<sub>0.17</sub>)<sub>3</sub>P NPs, (Cu<sub>0.83</sub>Co<sub>0.17</sub>)<sub>3</sub>P:S NPs and Pt/C in 0.5 M H<sub>2</sub>SO<sub>4</sub> electrolyte solution at 26 °C.**

Electro-catalyst	Lattice parameter (nm)	Molar volume (cm <sup>3</sup> mol <sup>-1</sup> )	Onset over potential (mV, RHE)	Overpotential (mV, RHE) to reach			Current density at (-0.05V) (mA cm <sup>-2</sup> )	R <sub>ct</sub> (Ω.cm <sup>2</sup> )
				10 mA cm <sup>-2</sup>	20 mA cm <sup>-2</sup>	100 mA cm <sup>-2</sup>		
Cu <sub>3</sub> P	a = b = 0.6959, c = 0.7413	31.20	190	519	813	>1048	0.01	65.29
(Cu <sub>0.83</sub> Co <sub>0.17</sub> ) <sub>3</sub> P	a = b = 0.6958, c = 0.7411	31.19	80	237	363	>809	0.085	31.3
(Cu <sub>0.83</sub> Co <sub>0.17</sub> ) <sub>3</sub> P:10S	a = b = 0.696, c = 0.7414	31.22	10	97	155	>567	3.19	21.29
(Cu <sub>0.83</sub> Co <sub>0.17</sub> ) <sub>3</sub> P:20S	a = b = 0.6962, c = 0.7415	31.24	10	52	70	185	8.67	10.31
(Cu <sub>0.83</sub> Co <sub>0.17</sub> ) <sub>3</sub> P:30S	a = b = 0.6963, c = 0.7417	31.26	10	46	58	105	17.2	7.00
Pt/C	–	–	10	43	51	95	17.6	6.32

(~778.4 eV) [28] and the peak at ~129.5 eV in the P 2p region of (Cu<sub>0.83</sub>Co<sub>0.17</sub>)<sub>3</sub>P:30S NPs (Fig. 3b) is at lower binding energies than that of elemental P (~130.2 eV) [69], respectively. Similar to the discussion above for pure Cu<sub>3</sub>P NPs, this also suggests the presence of Co (metal centers) with positive partial charge ( $\delta^+$ ) and P and S (pendant bases) with negative partial charge ( $\delta^-$ ) close to metal center and thus, implying transfer of electrons from Co to P and S in (Cu<sub>0.83</sub>Co<sub>0.17</sub>)<sub>3</sub>P:30S NPs and possible modification of the resulting charge density.

The XPS spectrum of (Cu<sub>0.83</sub>Co<sub>0.17</sub>)<sub>3</sub>P:30S NPs in the S 2p region (Fig. 3d) shows one peak at ~161 eV corresponding to the sulfide (S<sup>2-</sup>) showing no presence of any oxidized sulfur species such as sulfate (whose peak appears in S 2p<sub>3/2</sub> region at ~168 eV) [72,73]. The proton relays are incorporated in a metal complex electro-catalyst for HER arising from the pendant acid-base groups which are present close to the metal center where the HER is known to occur [20,74,75]. The active sites for metal complex hydrogenase enzyme also have pendant bases which are close to the metal centers [20,76]. The (Cu<sub>0.83</sub>Co<sub>0.17</sub>)<sub>3</sub>P:30S NPs considered in this study exhibit metal centers Cu, Co ( $\delta^+$ ) and pendant bases P, S ( $\delta^-$ ) positioned close to the metal centers [20]. Thus, (Cu<sub>0.83</sub>Co<sub>0.17</sub>)<sub>3</sub>P:30S NPs considered herein is expected to exhibit hydrogen evolution mechanism for HER similar to that of the metal complex hydrogenase enzyme reported [20]. Accordingly, Cu, Co and P, S in (Cu<sub>0.83</sub>Co<sub>0.17</sub>)<sub>3</sub>P:30S NPs can offer hydride-acceptor and proton-acceptor centers, respectively [20]. These results collectively thus, show modification of the electronic structure of Cu<sub>3</sub>P due to incorporation of Co and S into the lattice of the parent phosphide, Cu<sub>3</sub>P which can likely result in a more catalytically active phase offering superior electrochemical response compared to that of pure Cu<sub>3</sub>P NPs.

#### Electrochemical characterization of Cu<sub>3</sub>P, (Cu<sub>0.83</sub>Co<sub>0.17</sub>)<sub>3</sub>P and (Cu<sub>0.83</sub>Co<sub>0.17</sub>)<sub>3</sub>P:x at % S NPs (x = 10, 20, 30) compositions for HER in electrolytic water splitting

The electrochemical activity of Cu<sub>3</sub>P, (Cu<sub>0.83</sub>Co<sub>0.17</sub>)<sub>3</sub>P and (Cu<sub>0.83</sub>Co<sub>0.17</sub>)<sub>3</sub>P:S NPs of different S concentration has been studied by performing linear scan voltammetry in 0.5 M H<sub>2</sub>SO<sub>4</sub> electrolyte solution at 26 °C using a total loading of 0.7 mg cm<sup>-2</sup>. The *i*R<sub>Ω</sub> corrected LSV curves of commercial Pt/C (Pt loading = 0.4 mg<sub>Pt</sub> cm<sup>-2</sup>) and Ti foil (current collector) are shown in Fig. 4a. The Ti foil (current collector) as expected

shows very poor electrochemical activity for HER and thus, has minimal contribution to the current density obtained in comparison to other active electro-catalysts used in this study. The onset of HER starts at ~80 mV (*vs* RHE) for (Cu<sub>0.83</sub>Co<sub>0.17</sub>)<sub>3</sub>P NPs which is lower than that of pure Cu<sub>3</sub>P NPs (~190 mV *vs* RHE that is similar to earlier report [41]) (Table 2). This clearly suggests a reduction in the reaction polarization [7,9,11] due to the incorporation of cobalt into the Cu<sub>3</sub>P lattice which is in agreement with the results of theoretical study discussed earlier (Fig. 1). Following incorporation of sulfur for all the compositions considered in the current study, the NPs of the (Cu<sub>0.83</sub>Co<sub>0.17</sub>)<sub>3</sub>P:S system all show excellent performance for HER with an onset overpotential of ~10 mV (*vs* RHE). This response is not only similar to that of commercial Pt/C (Fig. 4a and Table 2) but also significantly lower than that of pure Cu<sub>3</sub>P NPs (~190 mV *vs* RHE). Thus, simultaneous incorporation of S and Co into the Cu<sub>3</sub>P lattice offers significant reduction in the onset overpotential of HER to the extent of ~180 mV (significantly reduced reaction polarization) and also offers reaction polarization similar to that of commercial Pt/C (similar onset overpotential). These results correlate well with results of theoretical study (discussed earlier) which predicts a minimum reaction polarization for (Cu<sub>0.83</sub>Co<sub>0.17</sub>)<sub>3</sub>P:S than that of pure Cu<sub>3</sub>P, due to the modification of the electronic structure following the simultaneous incorporation of Co and S into the Cu<sub>3</sub>P lattice. It is also important to note that the onset overpotential for HER (~10 mV *vs* HER) obtained in this study for (Cu<sub>0.83</sub>Co<sub>0.17</sub>)<sub>3</sub>P:30S NPs is the lowest onset overpotential obtained for HER thus far in the published open literature to date, compared to other reported non-noble metals based HER electro-catalysts, to the best of our knowledge (Table S1). This shows the excellent promise of Co and S acting as effective dopants in improving the electrochemical activity of the parent phosphide, Cu<sub>3</sub>P.

Nanoparticles (NP) of (Cu<sub>0.83</sub>Co<sub>0.17</sub>)<sub>3</sub>P exhibit current density of ~0.085 mA cm<sup>-2</sup> at (-0.05 V *vs* RHE, which is a finite potential required to overcome overpotential losses near 0V, standard potential of HER), the standard representative potential selected following literature reports for measuring electrochemical activity for HER [20,32,34,77–83]. which is eight-fold higher than that of pure Cu<sub>3</sub>P NPs (~0.01 mA cm<sup>-2</sup>) (Fig. 4a and Table 2). Additionally, (Cu<sub>0.83</sub>Co<sub>0.17</sub>)<sub>3</sub>P NPs show an overpotential of (>809 mV) (*vs* RHE) to reach a current density

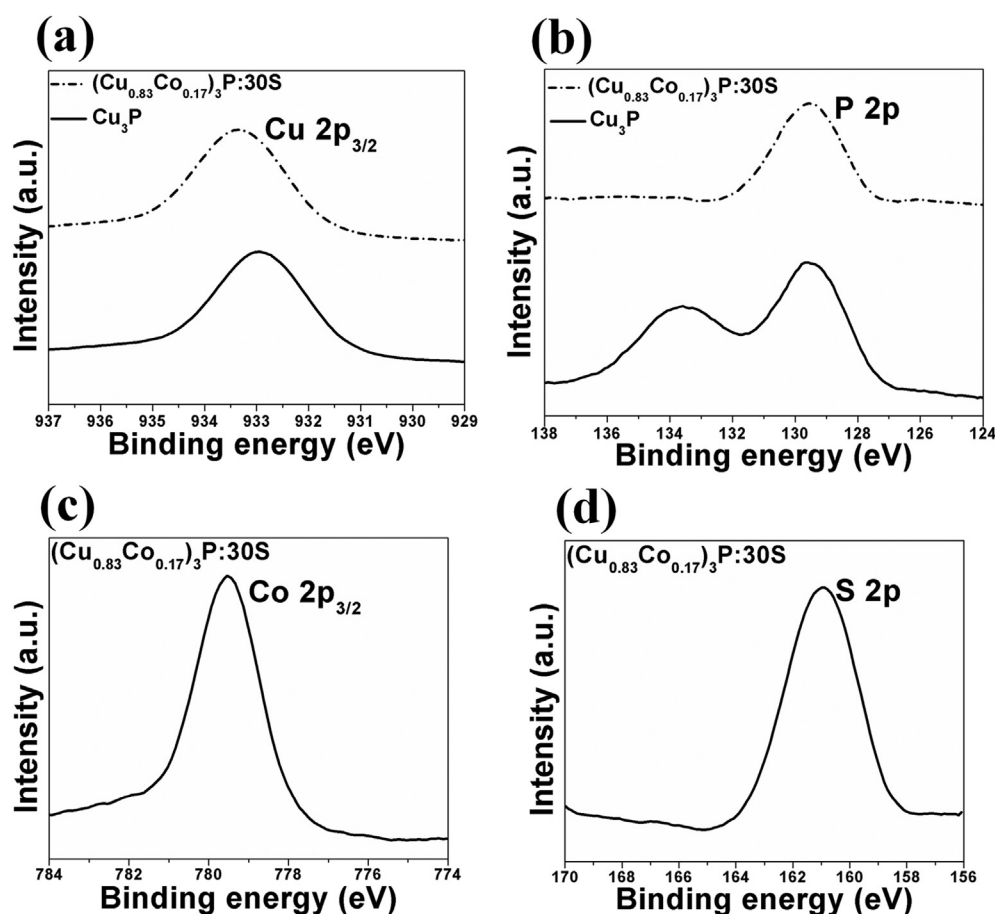
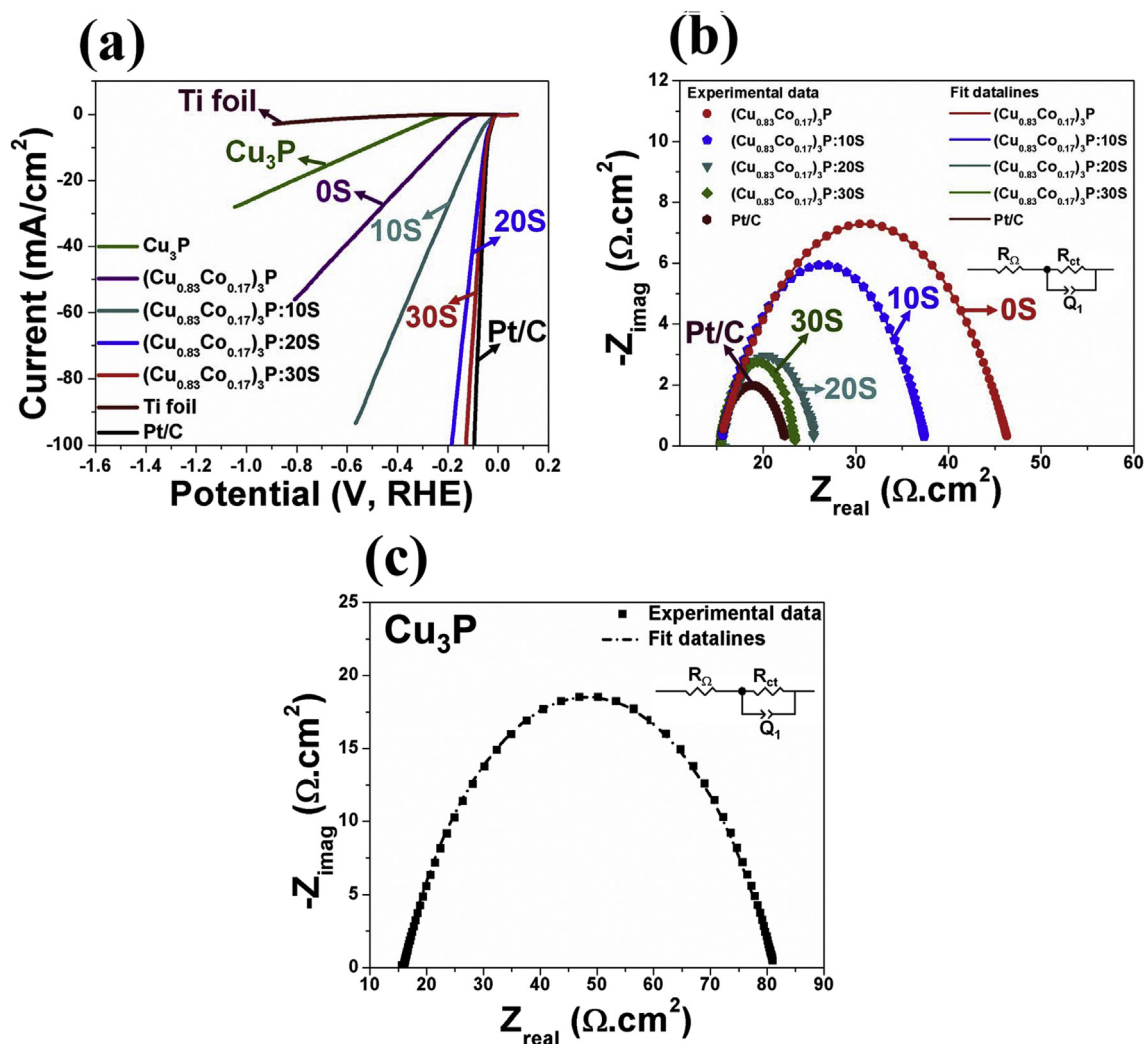


Fig. 3 – The XPS spectra of pure  $\text{Cu}_3\text{P}$  NPs and  $(\text{Cu}_{0.83}\text{Co}_{0.17})_3\text{P}:30\text{S}$  NPs in the (a)  $\text{Cu } 2p_{3/2}$  region, (b)  $\text{P } 2p$  region, (c)  $\text{Co } 2p_{3/2}$  region (d)  $\text{S } 2p$  region.

of  $100 \text{ mA cm}^{-2}$  which is lower than that of pure  $\text{Cu}_3\text{P}$  NPs showing an overpotential of ( $>1048 \text{ mV}$ ) (*vs* RHE) to reach the current density of  $100 \text{ mA cm}^{-2}$ , respectively (Fig. 4a and Table 2). This improvement in overpotential is mainly due to  $\sim 110 \text{ mV}$  lower onset overpotential (lower reaction polarization) and improved reaction kinetics (lower activation polarization) [7,9,11], also confirmed by the Electrochemical Impedance Spectroscopy (EIS) analysis discussed later) of  $(\text{Cu}_{0.83}\text{Co}_{0.17})_3\text{P}$  NPs (onset overpotential =  $\sim 80 \text{ mV vs RHE}$ ) than that of pure  $\text{Cu}_3\text{P}$  NPs (onset overpotential =  $\sim 190 \text{ mV vs RHE}$ ) (Fig. 4a and Table 2). However, despite this improvement, the current density of the  $(\text{Cu}_{0.83}\text{Co}_{0.17})_3\text{P}$  NPs at ( $-0.05 \text{ V vs RHE}$ ) ( $\sim 0.085 \text{ mA cm}^{-2}$ ) is  $\sim 99.5\%$  lower than that of Pt/C ( $\sim 17.6 \text{ mA cm}^{-2}$ ) and correspondingly, the overpotential required to reach the current density of  $100 \text{ mA cm}^{-2}$  is higher than that of commercial Pt/C which shows an overpotential of  $\sim 95 \text{ mV}$  (*vs* RHE, similar to earlier reports [20,32,34,78–83]) to reach the identical current density of  $100 \text{ mA cm}^{-2}$ , respectively (Fig. 4a and Table 2). This is mainly due to  $\sim 70 \text{ mV}$  higher onset overpotential and poor reaction kinetics of  $(\text{Cu}_{0.83}\text{Co}_{0.17})_3\text{P}$  NPs than that of commercial Pt/C (Fig. 4a and Table 2).

It is also important to note that the NPs in the  $(\text{Cu}_{0.83}\text{Co}_{0.17})_3\text{P}: \text{S}$  system exhibit almost two-orders of

magnitude higher current density at ( $-0.05 \text{ V vs RHE}$ ) than that of pure  $\text{Cu}_3\text{P}$  NPs and the Co doped phosphide,  $(\text{Cu}_{0.83}\text{Co}_{0.17})_3\text{P}$  NPs (Fig. 4a and Table 2). This result is indeed in agreement with the results of the theoretical study (as discussed above) and is a reflection of the significant reduction in reaction polarization and possibly lower activation polarization for  $(\text{Cu}_{0.83}\text{Co}_{0.17})_3\text{P}: \text{S}$  than that of pure  $\text{Cu}_3\text{P}$ . The current density at ( $-0.05 \text{ V vs RHE}$ ) for the NPs of the  $(\text{Cu}_{0.83}\text{Co}_{0.17})_3\text{P}: \text{S}$  system increases with increase in S dopant concentration with the highest current density value obtained for  $(\text{Cu}_{0.83}\text{Co}_{0.17})_3\text{P}:30\text{S}$  NPs ( $\sim 17.2 \text{ mA cm}^{-2}$ ) (Fig. 4a and Table 2). In addition, the overpotential required to reach the current density of  $100 \text{ mA cm}^{-2}$  for all of the sulfur doped  $(\text{Cu}_{0.83}\text{Co}_{0.17})_3\text{P}: \text{S}$  NPs decreases with increase in S concentration with the lowest value of  $105 \text{ mV}$  obtained for  $(\text{Cu}_{0.83}\text{Co}_{0.17})_3\text{P}:30\text{S}$  NPs (Fig. 4a and Table 2). Thus, despite the onset overpotential of  $(\text{Cu}_{0.83}\text{Co}_{0.17})_3\text{P}: \text{S}$  NPs of different S concentration being same ( $\sim 10 \text{ mV vs RHE}$ ), the increase in electrochemical activity of the sulfur doped  $(\text{Cu}_{0.83}\text{Co}_{0.17})_3\text{P}: \text{S}$  NPs with increase in S concentration with the highest activity displayed by  $(\text{Cu}_{0.83}\text{Co}_{0.17})_3\text{P}:30\text{S}$  NPs indicates improvement in reaction kinetics (decrease in activation polarization) with increase in S concentration with the highest obtained for  $(\text{Cu}_{0.83}\text{Co}_{0.17})_3\text{P}:30\text{S}$  NPs. The sulfur doped composition of



**Fig. 4** – (a) The  $iR_{\Omega}$  corrected linear scan voltammogram (LSV) curves for HER of pure  $\text{Cu}_3\text{P}$  NPs,  $(\text{Cu}_{0.83}\text{Co}_{0.17})_3\text{P}$  NPs,  $(\text{Cu}_{0.83}\text{Co}_{0.17})_3\text{P}:\text{S}$  NPs of different S concentration, Ti foil (current collector) and commercial Pt/C, obtained in 0.5 M  $\text{H}_2\text{SO}_4$  electrolyte solution at 26 °C using scan rate of  $1 \text{ mV s}^{-1}$ , (b) EIS spectra of  $(\text{Cu}_{0.83}\text{Co}_{0.17})_3\text{P}$  NPs,  $(\text{Cu}_{0.83}\text{Co}_{0.17})_3\text{P}:\text{S}$  NPs of different S concentration and commercial Pt/C obtained at  $(-0.05 \text{ V vs RHE})$  in 0.5 M  $\text{H}_2\text{SO}_4$  electrolyte solution at 26 °C in the frequency range of 100 mHz to 100 kHz (Amplitude = 10 mV), (c) EIS spectrum of  $\text{Cu}_3\text{P}$  NPs obtained at  $(-0.05 \text{ V vs RHE})$  in 0.5 M  $\text{H}_2\text{SO}_4$  electrolyte solution at 26 °C in the frequency range of 100 mHz to 100 kHz (Amplitude = 10 mV).

$(\text{Cu}_{0.83}\text{Co}_{0.17})_3\text{P}:\text{S}$  NPs show a current density of  $\sim 17.2 \text{ mA cm}^{-2}$  at  $(-0.05 \text{ V vs RHE})$  and overpotential of  $\sim 105 \text{ mV}$  (vs RHE) to reach the current density of  $100 \text{ mA cm}^{-2}$ , which is almost comparable to that of Pt/C (Fig. 4a and Table 2). Thus, the sulfur doped composition of  $(\text{Cu}_{0.83}\text{Co}_{0.17})_3\text{P}:\text{S}$  NPs display outstanding electrochemical performance for HER, almost comparable to that of commercial Pt/C (Fig. 4a and Table 2) which is due to similar reaction polarization and similar activation polarization for  $(\text{Cu}_{0.83}\text{Co}_{0.17})_3\text{P}:\text{S}$  NPs and commercial Pt/C. It is noteworthy that the overpotential of  $\sim 105 \text{ mV}$  (vs RHE) shown by  $(\text{Cu}_{0.83}\text{Co}_{0.17})_3\text{P}:\text{S}$  NPs to reach current density of  $100 \text{ mA cm}^{-2}$  in acidic media in this study is the lowest obtained so far compared to other reported non-noble metals based HER electro-catalysts, to the best of our knowledge (Table S1).

All of the NPs in the  $(\text{Cu}_{0.83}\text{Co}_{0.17})_3\text{P}:\text{S}$  show excellent electrochemical performance, even in neutral and basic media. The  $iR_{\Omega}$  corrected LSV curves of  $(\text{Cu}_{0.83}\text{Co}_{0.17})_3\text{P}:\text{S}$  NPs and Pt/C in 1 M potassium phosphate buffer (pH 7) and 1 M KOH (pH 14) are shown in Figs. S1 and S2 (Supporting information), respectively. It is clearly noticeable that all of the NPs in the  $(\text{Cu}_{0.83}\text{Co}_{0.17})_3\text{P}:\text{S}$  system show similar onset overpotential (similar reaction polarization) for HER as that of commercial Pt/C ( $\sim 10 \text{ mV vs RHE}$ ) in both neutral and basic media (Table S2 and Table S3). The current density at  $(-0.05 \text{ V vs RHE})$ , the potential selected to overcome overpotential losses near 0V standard potential of HER and once again following literature reports as accepted standard for electrochemical activity for HER [20,32,34,77–83] for all of the NPs in the  $(\text{Cu}_{0.83}\text{Co}_{0.17})_3\text{P}:\text{S}$  system increases with increase in S

concentration with the highest values of  $5.1 \text{ mA cm}^{-2}$  and  $3.55 \text{ mA cm}^{-2}$  obtained for  $(\text{Cu}_{0.83}\text{Co}_{0.17})_3\text{P}:30\text{S}$  NPs in both neutral and alkaline pH, respectively. Correspondingly, the overpotential required to reach the current density of  $100 \text{ mA cm}^{-2}$  for all the NPs in the  $(\text{Cu}_{0.83}\text{Co}_{0.17})_3\text{P}$ : S system decreases with increase in S concentration and the lowest values of 382 mV and 540 mV in neutral and alkaline pH, respectively obtained for  $(\text{Cu}_{0.83}\text{Co}_{0.17})_3\text{P}$ : 30S NPs in both neutral and basic media (Fig. S1–S2, Table S2 and Table S3 in Supporting information). Thus, the electrochemical activity for HER of NPs in the  $(\text{Cu}_{0.83}\text{Co}_{0.17})_3\text{P}$ : S system increases with increase in S concentration in both neutral and basic media similar to the acidic media with the highest response obtained for  $(\text{Cu}_{0.83}\text{Co}_{0.17})_3\text{P}:30\text{S}$  NPs in both neutral and basic media. As mentioned above, the  $(\text{Cu}_{0.83}\text{Co}_{0.17})_3\text{P}:30\text{S}$  NPs show excellent performance for HER in neutral media with current density at  $(-0.05 \text{ V vs RHE})$  ( $\sim 5.1 \text{ mA cm}^{-2}$ ) and the overpotential ( $\sim 382 \text{ mV vs RHE}$ ) required to reach current density of  $100 \text{ mA cm}^{-2}$  both of which are almost comparable to that of commercial Pt/C ( $\sim 330 \text{ mV vs RHE}$ ; similar to earlier reports [32]) (Fig. S1 and Table S2). Additionally, in basic media, the  $(\text{Cu}_{0.83}\text{Co}_{0.17})_3\text{P}:30\text{S}$  NPs exhibit excellent electrochemical activity for HER with current density at  $(-0.05 \text{ V vs RHE})$  ( $\sim 3.55 \text{ mA cm}^{-2}$ ) and similarly, the overpotential required to reach current density of  $100 \text{ mA cm}^{-2}$  comparable to that of commercial Pt/C ( $\sim 3.8 \text{ mA cm}^{-2}$  at  $-0.05 \text{ V vs RHE}$ ) (Fig. S2 and Table S3). It is also noteworthy to note that the overpotential shown by  $(\text{Cu}_{0.83}\text{Co}_{0.17})_3\text{P}:30\text{S}$  NPs to reach current density of  $100 \text{ mA cm}^{-2}$  in both, neutral and basic media reported in this study is the lowest obtained so far compared to other reported non-noble metals based HER electro-catalysts, to the best of our knowledge (Table S4 and Table S5). The above results clearly suggest that the introduction of Co and S as co-dopants in the  $\text{Cu}_3\text{P}$  lattice offer a synergistic alteration of the electronic, atomic/molecular structure (which is in agreement with results of theoretical study) leading to excellent electrochemical performance for HER, almost comparable to that of commercial Pt/C.

#### Electrochemical impedance spectroscopy and Tafel slopes

Based on the above, the reaction kinetics of HER for NPs of  $\text{Cu}_3\text{P}$ ,  $(\text{Cu}_{0.83}\text{Co}_{0.17})_3\text{P}$ , and for the various sulfur doped NPs in the  $(\text{Cu}_{0.83}\text{Co}_{0.17})_3\text{P}:S$  system including commercial Pt/C were studied using electrochemical impedance spectroscopy (EIS). Accordingly, EIS was carried out to determine the charge transfer resistance ( $R_{ct}$ ) in  $0.5 \text{ M H}_2\text{SO}_4$  electrolyte solution (pH=0) at  $(-0.05 \text{ V vs RHE})$  in the frequency range of 100 mHz–100 kHz at  $26^\circ\text{C}$  at an amplitude of 10 mV, using the circuit model  $R_o(R_{ct}Q_1)$  for fitting the experimental data, where  $R_o$  is the ohmic resistance, which includes contribution mainly from electrolyte and electrode. Similarly,  $R_{ct}$  is charge transfer resistance and  $Q_1$  is the constant phase element representing the contribution from the capacitance behavior of the electro-catalyst surface.

The EIS plot of the electro-catalysts show a well-formed semicircular arc (Fig. 4b–c). The diameter of semi-circular arc is used to determine the charge transfer resistance ( $R_{ct}$ ). The  $R_{ct}$  for all the NPs of the  $(\text{Cu}_{0.83}\text{Co}_{0.17})_3\text{P}$ : S system is

significantly lower than that of  $(\text{Cu}_{0.83}\text{Co}_{0.17})_3\text{P}$  NPs and pure  $\text{Cu}_3\text{P}$  NPs (Fig. 4b–c and Table 2) clearly reflecting significant improvements in the kinetics of HER (significant decrease in activation polarization) upon the incorporation of the dual dopants, Co and S into the  $\text{Cu}_3\text{P}$  lattice resulting in superior electrochemical activity for HER of all the NPs in the  $(\text{Cu}_{0.83}\text{Co}_{0.17})_3\text{P}:S$  system contrasted to that of  $(\text{Cu}_{0.83}\text{Co}_{0.17})_3\text{P}$  NPs and pure  $\text{Cu}_3\text{P}$  NPs, respectively. Correspondingly, the  $R_{ct}$  for all the NPs of the  $(\text{Cu}_{0.83}\text{Co}_{0.17})_3\text{P}:S$  system decreases with increase in S concentration with the lowest value of  $R_{ct}$  obtained for  $(\text{Cu}_{0.83}\text{Co}_{0.17})_3\text{P}:30\text{S}$  NPs ( $\sim 7 \Omega \text{ cm}^2$ ), suggesting improvement in reaction kinetics (decrease in activation polarization) and thus, improved electrochemical activity, with increase in S concentration with the highest current value of  $17.2 \text{ mA cm}^{-2}$  at  $-0.05 \text{ V vs RHE}$  obtained for  $(\text{Cu}_{0.83}\text{Co}_{0.17})_3\text{P}:30\text{S}$  NPs (exhibiting lowest activation polarization in this study) (Fig. 4b–c and Table 2). It should also be noted that  $R_{ct}$  for  $(\text{Cu}_{0.83}\text{Co}_{0.17})_3\text{P}:30\text{S}$  NPs ( $\sim 7 \Omega \text{ cm}^2$ ) is nine-fold lower than that of  $\text{Cu}_3\text{P}$  NPs ( $\sim 65.29 \Omega \text{ cm}^2$ ), five-fold lower than that of  $(\text{Cu}_{0.83}\text{Co}_{0.17})_3\text{P}$  NPs ( $\sim 31.3 \Omega \text{ cm}^2$ ) and almost comparable to commercial Pt/C ( $\sim 6.32 \Omega \text{ cm}^2$ ) (Fig. 4b–c and Table 2). Thus,  $(\text{Cu}_{0.83}\text{Co}_{0.17})_3\text{P}:30\text{S}$  NPs shows outstanding electrochemical performance for HER with the reaction kinetics (activation polarization) being almost similar to that of Pt/C.

The Tafel slope of pure  $\text{Cu}_3\text{P}$  NPs,  $(\text{Cu}_{0.83}\text{Co}_{0.17})_3\text{P}$  NPs,  $(\text{Cu}_{0.83}\text{Co}_{0.17})_3\text{P}:10\text{S}$  NPs,  $(\text{Cu}_{0.83}\text{Co}_{0.17})_3\text{P}:20\text{S}$  NPs and  $(\text{Cu}_{0.83}\text{Co}_{0.17})_3\text{P}:30\text{S}$  NPs and commercial Pt/C, calculated from  $iR_o$  corrected Tafel plots (in  $0.5 \text{ M H}_2\text{SO}_4$ ), are  $96 \text{ mV dec}^{-1}$ ,  $55 \text{ mV dec}^{-1}$ ,  $50 \text{ mV dec}^{-1}$ ,  $40 \text{ mV dec}^{-1}$ ,  $32 \text{ mV dec}^{-1}$  and  $31.6 \text{ mV dec}^{-1}$  (similar to earlier reports [32,78,79,82,84]), respectively (Fig. 5a–c). The lower Tafel slopes for all the NPs of the  $(\text{Cu}_{0.83}\text{Co}_{0.17})_3\text{P}$ : S system corresponding to different S concentrations compared to that of pure  $\text{Cu}_3\text{P}$  NPs and  $(\text{Cu}_{0.83}\text{Co}_{0.17})_3\text{P}$  NPs is again a reflection of the superior reaction kinetics of all the NPs of the  $(\text{Cu}_{0.83}\text{Co}_{0.17})_3\text{P}$ : S system than that of pure  $\text{Cu}_3\text{P}$  NPs and  $(\text{Cu}_{0.83}\text{Co}_{0.17})_3\text{P}$  NPs which is also seen in EIS analysis (Fig. 4b–c). The Tafel slope for  $(\text{Cu}_{0.83}\text{Co}_{0.17})_3\text{P}$ : S NPs decreases with increase in S concentration with the lowest value obtained for  $(\text{Cu}_{0.83}\text{Co}_{0.17})_3\text{P}:30\text{S}$  NPs ( $32 \text{ mV dec}^{-1}$ ), suggesting clearly an enhancement in the reaction kinetics (increase in number of electrons involved in HER) resulting in superior electrochemical activity for HER, which increases with increase in S concentration with the highest electrochemical response of  $17.2 \text{ mA cm}^{-2}$  at  $-0.05 \text{ V vs RHE}$  obtained for  $(\text{Cu}_{0.83}\text{Co}_{0.17})_3\text{P}:30\text{S}$  NPs (Fig. 5a–c). It is again of interest to note that the Tafel slope of  $(\text{Cu}_{0.83}\text{Co}_{0.17})_3\text{P}:30\text{S}$  NPs ( $32 \text{ mV dec}^{-1}$ ) is almost similar to that of commercial Pt/C ( $31.6 \text{ mV dec}^{-1}$ ) indicating almost similar reaction kinetics and thus, similar electrochemical activity of  $(\text{Cu}_{0.83}\text{Co}_{0.17})_3\text{P}:30\text{S}$  NPs and commercial Pt/C (Fig. 5a–c) for HER which is known to primarily proceed through the Volmer-Tafel mechanism for both  $(\text{Cu}_{0.83}\text{Co}_{0.17})_3\text{P}:30\text{S}$  NPs and commercial Pt/C [21,32]. The Tafel slope of  $(\text{Cu}_{0.83}\text{Co}_{0.17})_3\text{P}:30\text{S}$  NPs ( $32 \text{ mV dec}^{-1}$ ) is the lowest Tafel slope obtained so far compared to other reported non-noble metals based HER electro-catalysts published in the open literature, to the best of our knowledge (Table S1). These results collectively taken again show that the incorporation of dual dopants, Co and S into the  $\text{Cu}_3\text{P}$  lattice offers unique modification of the

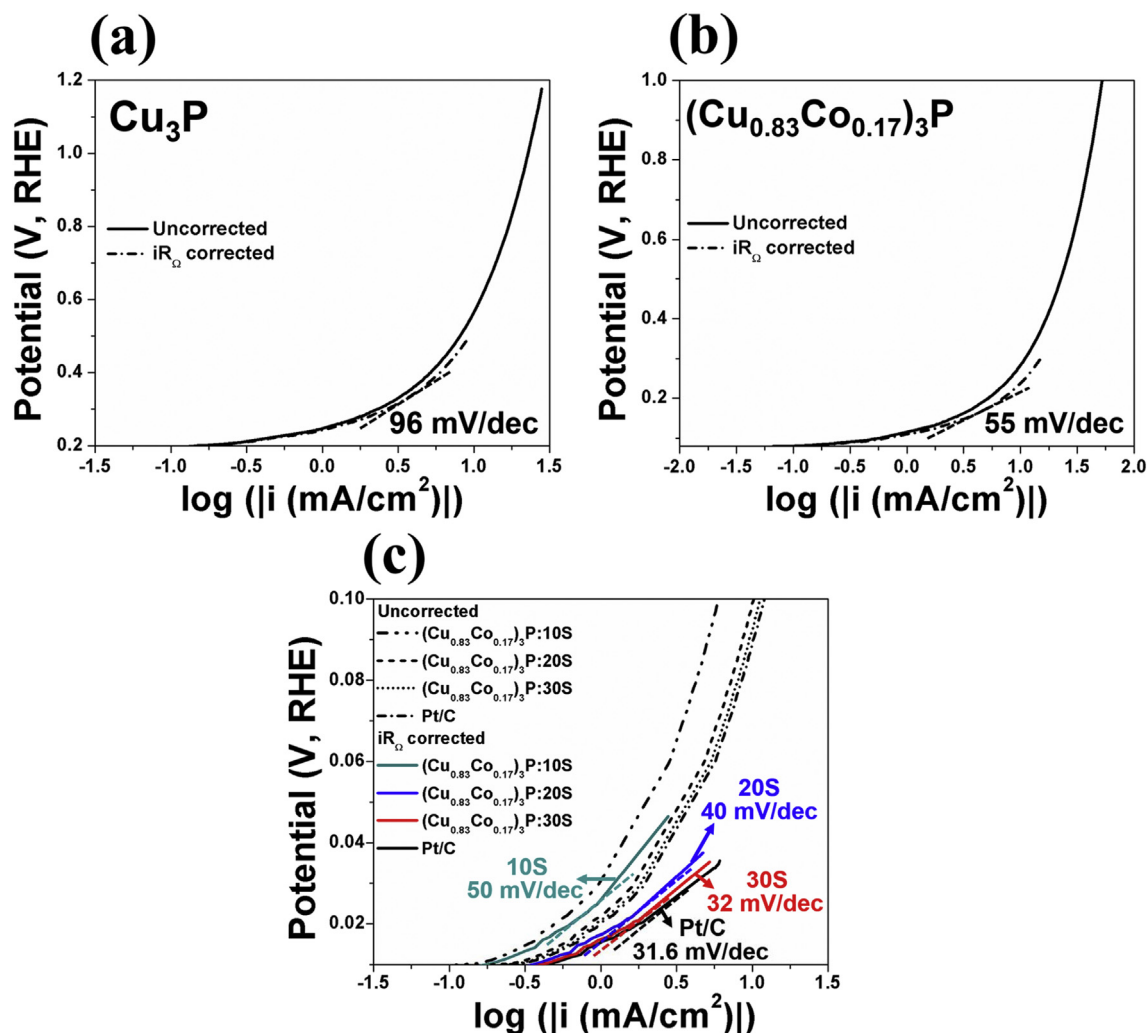


**Fig. 5** – (a) Tafel plot of pure  $\text{Cu}_3\text{P}$  NPs, (b) Tafel plot of  $(\text{Cu}_{0.83}\text{Co}_{0.17})_3\text{P}$  NPs, (c) Tafel plot of  $(\text{Cu}_{0.83}\text{Co}_{0.17})_3\text{P:S}$  NPs of different S concentration and commercial Pt/C.

electronic structure (as predicted by the first principles ab-initio studies discussed above and also seen in XPS analysis) exhibiting significantly lower reaction polarization and lower activation polarization than that of the parent  $\text{Cu}_3\text{P}$ , resulting in excellent electrochemical activity with the highest electrochemical activity of  $17.2 \text{ mA cm}^{-2}$  current density at  $-0.05 \text{ V}$  vs RHE obtained for  $(\text{Cu}_{0.83}\text{Co}_{0.17})_3\text{P:30S}$  NPs, which is almost similar to that of Pt/C ( $\sim 17.6 \text{ mA cm}^{-2}$ ).

#### Electrochemical stability test

The long term electrochemical stability of  $(\text{Cu}_{0.83}\text{Co}_{0.17})_3\text{P:30S}$  NPs is studied by performing chronoamperometry (CA) test wherein the electrode was maintained at constant potential of ( $-0.05 \text{ V}$  vs RHE) and the loss in current density (i.e., electrochemical activity) is studied for the period of 24 h. The CA curve of  $(\text{Cu}_{0.83}\text{Co}_{0.17})_3\text{P:30S}$  NPs, shown in Fig. 6a, alongside that of commercial Pt/C, depicts negligible loss in current density ( $\sim 1.6\%$ ) at the end of 24 h which is similar to that of commercial Pt/C ( $\sim 1.5\%$ ). The LSV curve obtained after 24 h of exposure of the  $(\text{Cu}_{0.83}\text{Co}_{0.17})_3\text{P:30S}$  NPs to the CA test (Fig. 6b) clearly depicts negligible loss in electrochemical activity. The

inductively coupled plasma optical emission spectroscopy (ICP-OES) analysis of electrolyte solution ( $0.5 \text{ M H}_2\text{SO}_4$ ) collected after 24 h of CA test of  $(\text{Cu}_{0.83}\text{Co}_{0.17})_3\text{P:30S}$  NPs indicates very minimal amount of elements ( $\sim 0$  ppm) having leached out from electrode in the electrolyte solution (Table S6). These results show excellent long term electrochemical stability of  $(\text{Cu}_{0.83}\text{Co}_{0.17})_3\text{P:30S}$  NPs, under HER operating conditions similar to that of Pt/C.

#### Electrochemical characterization of $(\text{Cu}_{0.83}\text{Co}_{0.17})_3\text{P:30S}$ NPs as HER electro-catalyst in H-type photoelectrochemical (PEC) water splitting cell using $(\text{Sn}_{0.95}\text{Nb}_{0.05})\text{O}_2\text{:N-600}$ nanotubes (NTs) as the photoanode

The NPs containing 30 at. % S, namely  $(\text{Cu}_{0.83}\text{Co}_{0.17})_3\text{P:30S}$  NPs is studied as electro-catalyst for HER in H-type PEC water splitting cell using  $(\text{Sn}_{0.95}\text{Nb}_{0.05})\text{O}_2\text{:N-600}$  nanotubes (NTs) as the photoanode/working electrode. The photoanode and cathode compartments were separated by Nafion 115 membrane in H-type cell [8]. Chronoamperometry (CA) test was conducted for  $(\text{Sn}_{0.95}\text{Nb}_{0.05})\text{O}_2\text{:N-600}$  NTs (photoanode) under illumination ( $100 \text{ mW cm}^{-2}$ ) by applying a constant potential of  $\sim 0.75 \text{ V}$  (vs RHE) for 24 h using  $(\text{Cu}_{0.83}\text{Co}_{0.17})_3\text{P:30S}$  NPs (total

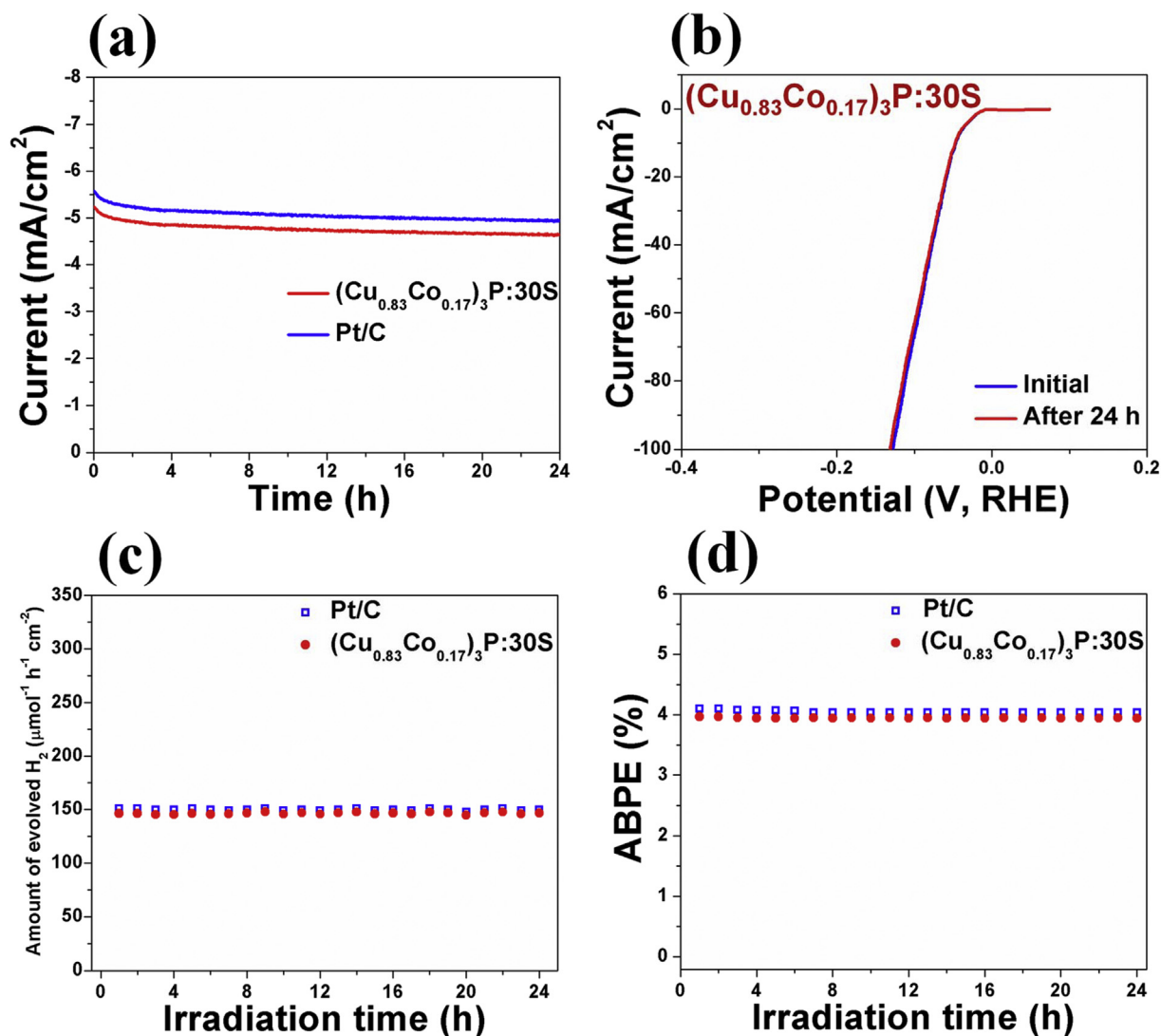


Fig. 6 – (a) The variation of current vs time in the chronoamperometry (CA) test of  $(\text{Cu}_{0.83}\text{Co}_{0.17})_3\text{P:30S}$  NPs and commercial Pt/C, performed in 0.5 M  $\text{H}_2\text{SO}_4$  electrolyte solution at a constant potential of  $(-0.05 \text{ V vs RHE})$  at  $26^\circ\text{C}$  for 24 h, (b) The  $iR_c$  corrected linear scan voltammogram (LSV) curve for HER of  $(\text{Cu}_{0.83}\text{Co}_{0.17})_3\text{P:30S}$  NPs, obtained in 0.5 M  $\text{H}_2\text{SO}_4$  electrolyte solution at  $26^\circ\text{C}$  using scan rate of  $1 \text{ mV s}^{-1}$ , before and after 24 h of CA test, (c) Amount of  $\text{H}_2$  evolved at cathode as a function of irradiation time for  $(\text{Cu}_{0.83}\text{Co}_{0.17})_3\text{P:30S}$  NPs and Pt/C as cathode electro-catalyst for HER and  $(\text{Sn}_{0.95}\text{Nb}_{0.05})\text{O}_2\text{:N-600}$  nanotubes (NTs) as photoanode/working electrode, obtained in 0.5 M  $\text{H}_2\text{SO}_4$  solution at  $26^\circ\text{C}$  under illumination ( $100 \text{ mW cm}^{-2}$ ) in chronomaperometry test of  $(\text{Sn}_{0.95}\text{Nb}_{0.05})\text{O}_2\text{:N-600}$  NTs performed at a constant potential of  $-0.75 \text{ V}$  (vs RHE) at  $26^\circ\text{C}$  for 24 h, (d) Applied bias photon-to-current efficiency (ABPE) as a function of irradiation time for  $(\text{Cu}_{0.83}\text{Co}_{0.17})_3\text{P:30S}$  NPs and Pt/C as cathode electro-catalyst for HER and  $(\text{Sn}_{0.95}\text{Nb}_{0.05})\text{O}_2\text{:N-600}$  nanotubes (NTs) as photoanode/working electrode, obtained in 0.5 M  $\text{H}_2\text{SO}_4$  solution at  $26^\circ\text{C}$  under illumination ( $100 \text{ mW cm}^{-2}$ ) in chronomaperometry test of  $(\text{Sn}_{0.95}\text{Nb}_{0.05})\text{O}_2\text{:N-600}$  NTs performed at a constant potential of  $-0.75 \text{ V}$  (vs RHE) at  $26^\circ\text{C}$  for 24 h.

loading =  $0.7 \text{ mg cm}^{-2}$ ) as the cathode electro-catalyst for HER in 0.5 M  $\text{H}_2\text{SO}_4$  electrolyte solution (pH=0) at  $26^\circ\text{C}$ . It should be mentioned that  $0.75 \text{ V}$  (vs RHE) is chosen for the CA test, since a maximum ABPE of  $\sim 4.1\%$  was obtained using  $(\text{Sn}_{0.95}\text{Nb}_{0.05})\text{O}_2\text{:N-600}$  nanotubes (NTs) as semiconductor material for photoanode as mentioned earlier, and Pt as cathode electro-catalyst for HER, as well as reported by us in an earlier publication [8]). During the CA test, the amount of  $\text{H}_2$  gas (generated at the cathode) was measured after each 1 h interval using a gas chromatograph (helium as the carrier gas, Agilent 7820A)

and further used for the determination of the applied bias photon-to-current efficiency (ABPE). For comparison, the ABPE was also determined using Pt/C (Pt loading =  $0.4 \text{ mg}_{\text{Pt}} \text{ cm}^{-2}$ ) as the cathode electro-catalyst, using similar procedure followed for  $(\text{Cu}_{0.83}\text{Co}_{0.17})_3\text{P:30S}$  NPs.

The amount of  $\text{H}_2$  generated at the cathode as a function of irradiation time for  $(\text{Cu}_{0.83}\text{Co}_{0.17})_3\text{P:30S}$  NPs and Pt/C used as the cathode electro-catalyst, is shown in Fig. 6c. It is noteworthy to see that the amount of  $\text{H}_2$  evolved at the cathode using the 30 at. % S containing NPs of  $(\text{Cu}_{0.83}\text{Co}_{0.17})_3\text{P:30S}$  as

electro-catalyst is almost similar to that of commercial Pt/C. This can again be considered to be due to similar reaction polarization (similar onset overpotential) and similar activation polarization (similar reaction kinetics) for both  $(\text{Cu}_{0.83}\text{Co}_{0.17})_3\text{P}:3\text{OS}$  NPs and commercial Pt/C, as discussed earlier in the LSV studies (Fig. 4a and Table 2) and EIS analysis (Fig. 4b–c and Table 2). Correspondingly, the ABPE is determined using the equation [85–89]:

$$\text{ABPE} = \frac{\Delta G^\circ \cdot n_{\text{H}_2} - V \cdot I}{P \cdot A} \times 100$$

where,  $n_{\text{H}_2}$  =  $\text{H}_2$  evolution rate ( $\text{mol sec}^{-1}$ ).

$\Delta G^\circ$  = Gibbs free energy for generating 1 mol of  $\text{H}_2$  from water ( $237130 \text{ J mol}^{-1}$ ).

P = Total incident power ( $\text{W cm}^{-2}$ ).

A = Area irradiated by incident light ( $\text{cm}^2$ ).

I = Photocurrent (A).

V = Bias voltage applied (0.75 V vs RHE) to  $(\text{Sn}_{0.95}\text{Nb}_{0.05})\text{O}_2:\text{N}-600$  NTs (photoanode/working electrode).

The plot of ABPE as function of irradiation time is shown in Fig. 6d. The ABPE obtained using  $(\text{Cu}_{0.83}\text{Co}_{0.17})_3\text{P}:3\text{OS}$  NPs (~4%) is almost similar to that obtained using commercial Pt/C as cathode electro-catalyst for HER (~4.1%). Also, it should be noted that the ABPE of ~4% is obtained using materials (for both, the cathode and the photoanode) completely devoid of any precious metals (e.g. Pt) in this study. Furthermore, the ABPE of ~4% obtained using  $(\text{Cu}_{0.83}\text{Co}_{0.17})_3\text{P}:3\text{OS}$  NPs as HER electro-catalyst and  $(\text{Sn}_{0.95}\text{Nb}_{0.05})\text{O}_2:\text{N}-600$  NTs as photoanode in H-type PEC water splitting cell is the highest ABPE obtained thus far in the open published literature compared to other semiconductor materials studied as photoanode for PEC water splitting based on  $\text{TiO}_2$ ,  $\text{ZnO}$  and  $\text{Fe}_2\text{O}_3$  to the best of our knowledge [8,10,49–52]. In addition, the minimal loss in ABPE (~1.8%) for  $(\text{Cu}_{0.83}\text{Co}_{0.17})_3\text{P}:3\text{OS}$  NPs at the end of 24 h of irradiation shows excellent electrochemical stability of  $(\text{Cu}_{0.83}\text{Co}_{0.17})_3\text{P}:3\text{OS}$  NPs similar to that of Pt/C (~1.7% loss in ABPE at the end of 24 h) for continuous  $\text{H}_2$  production in the PEC water splitting cell used in the current study for both the  $(\text{Cu}_{0.83}\text{Co}_{0.17})_3\text{P}:3\text{OS}$  NPs and Pt/C system using  $(\text{Sn}_{0.95}\text{Nb}_{0.05})\text{O}_2:\text{N}-600$  NTs as the photoanode.

The present theoretical and experimental study demonstrates excellent electrochemical performance of  $(\text{Cu}_{0.83}\text{Co}_{0.17})_3\text{P}:3\text{OS}$  NPs, almost similar to that of commercial Pt/C in acidic, neutral and basic media. This can be attributed to the introduction of Co and S in the  $\text{Cu}_3\text{P}$  lattice, resulting in novel and unique modification of the electronic structure, as indicated by the first principle studies outlined earlier above (Fig. 1) and confirmed by XPS analysis (Fig. 3a–d). The system correspondingly exhibits onset overpotential as seen in LSV plot (Fig. 4a and Table 2), reaction kinetics (charge transfer resistance) as studied in EIS analysis (Fig. 4b–c and Table 2) and Tafel slope (Fig. 5a–c and Table 2), electrochemical activity in PEC water splitting cell in acidic media ( $\text{H}_2$  yield and ABPE) (Fig. 6c–d), almost similar to that of commercial Pt/C. These results collectively thus, demonstrate the potential of  $(\text{Cu}_{0.83}\text{Co}_{0.17})_3\text{P}:3\text{OS}$  NPs clearly as a replacement of the state of the art commercial Pt/C and with further system modification it is possible that the system can achieve even superior electrochemical activity for HER than that of Pt/C. A thorough fundamental study for  $(\text{Cu},\text{Co})_3\text{P}:\text{S}$  electro-catalyst material

involving DFT studies and experimental approaches for Co-doped  $\text{Cu}_3\text{P}$  with different Co content (10–50 at.%) and S-doped  $\text{Cu}_3\text{P}$  with different S content (10–50 at.%) to study the surface electronic structure, bulk electronic and electrochemical properties along with testing of the electro-catalysts in 2-electrode PEC water splitting system, long term stability assessment by chronopotentiometry test (at the overpotential of  $50 \text{ mA/cm}^2$ ,  $100 \text{ mA/cm}^2$  and  $200 \text{ mA/cm}^2$ ) and post-stability characterization analyses will be planned in the future and reported in the subsequent publications. The present report of its excellent electrochemical performance and stability for HER in both electrolytic water splitting (i.e., water electrolysis) and PEC water splitting indeed is a testimonial of a hallmark breakthrough achieved in the pursuit of identification and development of low cost, highly active and robust non-noble metals based electro-catalyst for HER for replacing the expensive state of the art commercial Pt/C electro-catalyst used at present.

## Conclusions

The present study shows that the sulfur and cobalt doped  $(\text{Cu}_{0.83}\text{Co}_{0.17})_3\text{P}:\text{S}$  nanoparticles (NPs) system serves as a potential cathode electro-catalyst for HER. The system was identified using theoretical first principles studies. The XRD patterns of the synthesized  $(\text{Cu}_{0.83}\text{Co}_{0.17})_3\text{P}:\text{S}$  NPs clearly indicate the formation of single phase with hexagonal structure (similar to that of  $\text{Cu}_3\text{P}$ ). The XPS analysis conducted also showed modification in the electronic structure upon incorporation of Co and S into the  $\text{Cu}_3\text{P}$  lattice, leading to superior electrochemical activity for HER. The present study thus clearly demonstrates  $(\text{Cu}_{0.83}\text{Co}_{0.17})_3\text{P}:\text{S}$  NPs of different S concentration exhibiting excellent electrochemical activity for HER with onset overpotential of ~10 mV (vs RHE) which is similar to that of commercial Pt/C in all three electrolyte conditions of acidic, neutral and basic media and is indeed the lowest obtained so far compared to other reported non-noble metals based HER electro-catalysts in the open literature. The highest electrochemical performance is obtained for  $(\text{Cu}_{0.83}\text{Co}_{0.17})_3\text{P}:3\text{OS}$  NPs, which showed overpotential to reach current density of  $100 \text{ mA cm}^{-2}$ , almost similar to that of commercial Pt/C in acidic, neutral and basic media and lower than other reported non-noble metals based HER electro-catalysts. These results bode well with the results of the theoretical study. Additionally, the  $(\text{Cu}_{0.83}\text{Co}_{0.17})_3\text{P}:3\text{OS}$  NPs showed excellent electrochemical activity for HER as cathode electro-catalyst in PEC water splitting system using  $(\text{Sn}_{0.95}\text{Nb}_{0.05})\text{O}_2:\text{N}-600$  nanotubes (NTs) as photoanode in acidic media. An ABPE of ~4% obtained using  $(\text{Cu}_{0.83}\text{Co}_{0.17})_3\text{P}:3\text{OS}$  NPs is almost similar to that of commercial Pt/C as cathode electro-catalyst for HER (~4.1%) and the highest obtained so far using completely non-noble metals based materials (for cathode and photoanodes based on literature reports for  $\text{TiO}_2$ ,  $\text{ZnO}$  and  $\text{Fe}_2\text{O}_3$ ), to the best of our knowledge. Furthermore, the  $(\text{Cu}_{0.83}\text{Co}_{0.17})_3\text{P}:3\text{OS}$  NPs exhibit excellent long term electrochemical stability for HER in acidic media similar to that of Pt/C in both water electrolysis and PEC water splitting cell. Hence, the present study demonstrates  $(\text{Cu}_{0.83}\text{Co}_{0.17})_3\text{P}:3\text{OS}$  NPs as potential electro-catalyst for

replacing Pt/C for HER in electrolytic and photoelectrochemical water splitting system due to its excellent electrochemical performance and stability. The results reported here is anticipated to offer significant reduction in the capital cost of electrolytic and PEC water splitting systems for achieving efficient and economic hydrogen generation to address the global energy crisis. It is also likely that this system will ensure sustainable development of modern society utilizing clean non-carbonaceous fuels leading to an energy efficient economy.

### Author contributions

P.P.P. and P.N.K. devised the original concept. P.P.P. designed the experiments, synthesized the electro-catalyst materials, prepared the electrodes, performed structural, electrochemical and photoelectrochemical characterization and analyzed electrochemical data. O.I.V. conducted the theoretical analyses. P.M.S. collected the XPS data. P.P.P. and B.G. performed SEM-EDX-elemental x-ray mapping and TEM analyses, respectively. P.P.P. analyzed the XPS data. M.K.D., R.K., S.D.G. and P.J. made suggestions to the draft components. P. P. P., O.I.V. and P.N.K. wrote the first draft of the paper and all authors participated in the manuscript review and revision. The project is conceived and supervised by P.N.K.

### Acknowledgments

Research supported by the U.S. Department of Energy, Office of Basic Energy Sciences, Division of Materials Sciences and Engineering under Award DE-SC0001531. PNK acknowledges the Edward R. Weidlein Chair Professorship funds, the Center for Complex Engineered Multifunctional Materials (CEMM) for procuring the electrochemical equipment and facilities used in this research work and the Pittsburgh Supercomputing Center for providing the computational resources. PNK also acknowledges the support of the National Science Foundation, CBET-Grant 0933141 and CBET-Grant 1511390. Finally, P.N.K. and O.I.V. gratefully acknowledge the Extreme Science and Engineering Discovery Environment (XSEDE) [90] supported by National Science Foundation grant number ACI-1053575, for providing the computational resources needed to complete the theoretical component of the present study.

### Appendix A. Supplementary data

Supplementary data related to this article can be found at <https://doi.org/10.1016/j.ijhydene.2018.02.147>.

### REFERENCES

- [1] Nowotny J, Bak T, Chu D, Fiechter S, Murch GE, Veziroglu TN. Sustainable practices: solar hydrogen fuel and education program on sustainable energy systems. *Int J Hydrogen Energy* 2014;39:4151–7.
- [2] Andrews J, Shabani B. The role of hydrogen in a global sustainable energy strategy. *Wiley Interdiscipl Rev: Energy Environ* 2014;3:474–89.
- [3] Marchenko OV, Solomin SV. The future energy: hydrogen versus electricity. *Int J Hydrogen Energy* 2015;40:3801–5.
- [4] Nicoletti G, Arcuri N, Nicoletti G, Bruno R. A technical and environmental comparison between hydrogen and some fossil fuels. *Energy Convers Manag* 2015;89:205–13.
- [5] Peters GP, Andrew RM, Boden T, Canadell JG, Ciais P, Le Quere C, et al. The challenge to keep global warming below 2 [deg]C. *Nat Clim Change* 2013;3:4–6.
- [6] Patel PP, Velikokhatnyi OI, Ghadge SD, Jampani PH, Datta MK, Hong D, et al. Highly active robust oxide solid solution electro-catalysts for oxygen reduction reaction for proton exchange membrane fuel cell and direct methanol fuel cell cathodes. *Int J Hydrogen Energy* 2017;42:24079–89.
- [7] Patel PP, Hanumantha PJ, Datta MK, Velikokhatnyi OI, Hong D, Poston JA, et al. WO<sub>3</sub> based solid solution oxide - promising proton exchange membrane fuel cell anode/electro-catalyst. *J Mater Chem* 2015;3:18296–309.
- [8] Patel PP, Hanumantha PJ, Velikokhatnyi OI, Datta MK, Gattu B, Poston JA, et al. Vertically aligned nitrogen doped (Sn,Nb)O<sub>2</sub> nanotubes – robust photoanodes for hydrogen generation by photoelectrochemical water splitting. *Mater Sci Eng: B* 2016;208:1–14.
- [9] Patel PP, Datta MK, Velikokhatnyi OI, Kuruba R, Damodaran K, Jampani P, et al. Noble metal-free bifunctional oxygen evolution and oxygen reduction acidic media electro-catalysts. *Sci Rep* 2016;6.
- [10] Patel PP, Hanumantha PJ, Velikokhatnyi OI, Datta MK, Hong D, Gattu B, et al. Nitrogen and cobalt co-doped zinc oxide nanowires – viable photoanodes for hydrogen generation via photoelectrochemical water splitting. *J Power Sources* 2015;299:11–24.
- [11] Patel PP, Datta MK, Velikokhatnyi OI, Jampani P, Hong D, Poston JA, et al. Nanostructured robust cobalt metal alloy based anode electro-catalysts exhibiting remarkably high performance and durability for proton exchange membrane fuel cells. *J Mater Chem* 2015;3:14015–32.
- [12] Patel PP, Datta MK, Jampani PH, Hong D, Poston JA, Manivannan A, et al. High performance and durable nanostructured TiN supported Pt<sub>50</sub>–Ru<sub>50</sub> anode catalyst for direct methanol fuel cell (DMFC). *J Power Sources* 2015;293:437–46.
- [13] Turner J, Sverdrup G, Mann MK, Maness PC, Kroposki B, Ghirardi M, et al. Renewable hydrogen production. *Int J Energy Res* 2008;32:379–407.
- [14] Kibsgaard J, Jaramillo TF. Molybdenum phosphosulfide: an active, acid-stable, earth-abundant catalyst for the hydrogen evolution reaction. *Angew Chem Int Ed* 2014;53:14433–7.
- [15] Crabtree GW, Dresselhaus MS, Buchanan MV. The hydrogen economy. *Phys Today* 2004;57:39–44.
- [16] Bard AJ, Fox MA. Artificial photosynthesis: solar splitting of water to hydrogen and oxygen. *Accounts Chem Res* 1995;28:141–5.
- [17] Winter C-J. Hydrogen energy—abundant, efficient, clean: a debate over the energy-system-of-change. *Int J Hydrogen Energy* 2009;34:S1–S2.
- [18] Coelho B, Oliveira A, Mendes A. Concentrated solar power for renewable electricity and hydrogen production from water—a review. *Energy Environ Sci* 2010;3:1398–405.
- [19] Chen X, Shen S, Guo L, Mao SS. Semiconductor-based photocatalytic hydrogen generation. *Chem Rev* 2010;110:6503–70.

[1] Nowotny J, Bak T, Chu D, Fiechter S, Murch GE, Veziroglu TN. Sustainable practices: solar hydrogen fuel and education

- [20] Tian J, Liu Q, Asiri AM, Sun X. Self-supported nanoporous cobalt phosphide nanowire arrays: an efficient 3D hydrogen-evolving cathode over the wide range of pH 0–14. *J Am Chem Soc* 2014;136:7587–90.
- [21] Li Y, Wang H, Xie L, Liang Y, Hong G, Dai H. MoS<sub>2</sub> nanoparticles grown on graphene: an advanced catalyst for the hydrogen evolution reaction. *J Am Chem Soc* 2011;133:7296–9.
- [22] Hinnemann B, Moses PG, Bonde J, Jørgensen KP, Nielsen JH, Hørch S, et al. Biomimetic hydrogen evolution: MoS<sub>2</sub> nanoparticles as catalyst for hydrogen evolution. *J Am Chem Soc* 2005;127:5308–9.
- [23] Kong D, Wang H, Lu Z, Cui Y. CoSe<sub>2</sub> nanoparticles grown on carbon fiber paper: an efficient and stable electrocatalyst for hydrogen evolution reaction. *J Am Chem Soc* 2014;136:4897–900.
- [24] Cao B, Veith GM, Neuefeind JC, Adzic RR, Khalifah PG. Mixed close-packed cobalt molybdenum nitrides as non-noble metal electrocatalysts for the hydrogen evolution reaction. *J Am Chem Soc* 2013;135:19186–92.
- [25] Tang H, Dou K, Kaun C-C, Kuang Q, Yang S. MoSe<sub>2</sub> nanosheets and their graphene hybrids: synthesis, characterization and hydrogen evolution reaction studies. *J Mater Chem* 2014;2:360–4.
- [26] Chen W-F, Sasaki K, Ma C, Frenkel AI, Marinkovic N, Muckerman JT, et al. Hydrogen-evolution catalysts based on non-noble metal nickel–molybdenum nitride nanosheets. *Angew Chem* 2012;124:6235–9.
- [27] Yang J, Voiry D, Ahn SJ, Kang D, Kim AY, Chhowalla M, et al. Two-dimensional hybrid nanosheets of tungsten disulfide and reduced graphene oxide as catalysts for enhanced hydrogen evolution. *Angew Chem* 2013;125:13996–9.
- [28] Jiang P, Liu Q, Ge C, Cui W, Pu Z, Asiri AM, et al. CoP nanostructures with different morphologies: synthesis, characterization and a study of their electrocatalytic performance toward the hydrogen evolution reaction. *J Mater Chem* 2014;2:14634–40.
- [29] Oyama ST, Gott T, Zhao H, Lee Y-K. Transition metal phosphide hydroprocessing catalysts: a review. *Catal Today* 2009;143:94–107.
- [30] Carenco S, Portehault D, Boissière C, Mézailles N, Sanchez C. Nanoscaled metal borides and phosphides: recent developments and perspectives. *Chem Rev* 2013;113:7981–8065.
- [31] Prins R, Bussell M. Metal phosphides: preparation, characterization and catalytic reactivity. *Catal Lett* 2012;142:1413–36.
- [32] Tian J, Liu Q, Liang Y, Xing Z, Asiri AM, Sun X. FeP nanoparticles film grown on carbon cloth: an ultrahighly active 3D hydrogen evolution cathode in both acidic and neutral solutions. *ACS Appl Mater Interfaces* 2014;6:20579–84.
- [33] Popczun EJ, McKone JR, Read CG, Biacchi AJ, Wiltrot AM, Lewis NS, et al. Nanostructured nickel phosphide as an electrocatalyst for the hydrogen evolution reaction. *J Am Chem Soc* 2013;135:9267–70.
- [34] Feng L, Vrabel H, Bensimon M, Hu X. Easily-prepared dinickel phosphide (Ni<sub>2</sub>P) nanoparticles as an efficient and robust electrocatalyst for hydrogen evolution. *Phys Chem Chem Phys* 2014;16:5917–21.
- [35] Popczun EJ, Roske CW, Read CG, Crompton JC, McEnaney JM, Callejas JF, et al. Highly branched cobalt phosphide nanostructures for hydrogen-evolution electrocatalysis. *J Mater Chem* 2015;3:5420–5.
- [36] Popczun EJ, Read CG, Roske CW, Lewis NS, Schaak RE. Highly active electrocatalysis of the hydrogen evolution reaction by cobalt phosphide nanoparticles. *Angew Chem* 2014;126:5531–4.
- [37] Xiao P, Sk MA, Thia L, Ge X, Lim RJ, Wang J-Y, et al. Molybdenum phosphide as an efficient electrocatalyst for the hydrogen evolution reaction. *Energy Environ Sci* 2014;7:2624–9.
- [38] Callejas JF, McEnaney JM, Read CG, Crompton JC, Biacchi AJ, Popczun EJ, et al. Electrocatalytic and photocatalytic hydrogen production from acidic and neutral-pH aqueous solutions using iron phosphide nanoparticles. *ACS Nano* 2014;8:11101–7.
- [39] McEnaney JM, Crompton JC, Callejas JF, Popczun EJ, Read CG, Lewis NS, et al. Electrocatalytic hydrogen evolution using amorphous tungsten phosphide nanoparticles. *Chem Commun* 2014;50:11026–8.
- [40] Xing Z, Liu Q, Asiri AM, Sun X. High-efficiency electrochemical hydrogen evolution catalyzed by tungsten phosphide submicroparticles. *ACS Catal* 2014;5:145–9.
- [41] Tian J, Liu Q, Cheng N, Asiri AM, Sun X. Self-supported Cu<sub>3</sub>P nanowire arrays as an integrated high-performance three-dimensional cathode for generating hydrogen from water. *Angew Chem Int Ed* 2014;53:9577–81.
- [42] Merki D, Vrabel H, Rovelli L, Fierro S, Hu X. Fe, Co, and Ni ions promote the catalytic activity of amorphous molybdenum sulfide films for hydrogen evolution. *Chem Sci* 2012;3:2515–25.
- [43] Bonde J, Moses PG, Jaramillo TF, Nørskov JK, Chorkendorff I. Hydrogen evolution on nano-particulate transition metal sulfides. *Faraday Discuss* 2009;140:219–31.
- [44] Okamoto Y, Tamura K, Kubota T. Edge-differentiating deposition of Co on SiO<sub>2</sub>-supported MoS<sub>2</sub> particles. *Chem Commun* 2010;46:2748–50.
- [45] Byskov LS, Nørskov JK, Clausen BS, Topsøe H. DFT calculations of unpromoted and promoted MoS<sub>2</sub>-based hydrodesulfurization catalysts. *J Catal* 1999;187:109–22.
- [46] Lauritsen JV, Helveg S, Lægsgaard E, Stensgaard I, Clausen BS, Topsøe H, et al. Atomic-scale structure of Co–Mo–S nanoclusters in hydrotreating catalysts. *J Catal* 2001;197:1–5.
- [47] Shu Y, Oyama ST. Synthesis, characterization, and hydrotreating activity of carbon-supported transition metal phosphides. *Carbon* 2005;43:1517–32.
- [48] Bai J, Li X, Wang A, Prins R, Wang Y. Different role of H<sub>2</sub>S and dibenzothiophene in the incorporation of sulfur in the surface of bulk MoP during hydrodesulfurization. *J Catal* 2013;300:197–200.
- [49] Cho IS, Chen Z, Forman AJ, Kim DR, Rao PM, Jaramillo TF, et al. Branched TiO<sub>2</sub> nanorods for photoelectrochemical hydrogen production. *Nano Lett* 2011;11:4978–84.
- [50] Wang G, Wang H, Ling Y, Tang Y, Yang X, Fitzmorris RC, et al. Hydrogen-treated TiO<sub>2</sub> nanowire arrays for photoelectrochemical water splitting. *Nano Lett* 2011;11:3026–33.
- [51] Dotan H, Sivula K, Gratzel M, Rothschild A, Warren SC. Probing the photoelectrochemical properties of hematite ([small alpha]-Fe<sub>2</sub>O<sub>3</sub>) electrodes using hydrogen peroxide as a hole scavenger. *Energy Environ Sci* 2011;4:958–64.
- [52] Liu Q, Ding D, Ning C, Wang X. Black Ni-doped TiO<sub>2</sub> photoanodes for high-efficiency photoelectrochemical water-splitting. *Int J Hydrogen Energy* 2015;40:2107–14.
- [53] Hammer B, Nørskov JK. Theoretical surface science and catalysis—calculations and concepts. *Adv Catal* 2000;45:71–129.
- [54] Bligaard T, Nørskov JK. Ligand effects in heterogeneous catalysis and electrochemistry. *Electrochim Acta* 2007;52:5512–6.
- [55] Nørskov JK, Bligaard T, Logadottir A, Kitchin J, Chen J, Pandelov S, et al. Trends in the exchange current for hydrogen evolution. *J Electrochem Soc* 2005;152:J23–6.
- [56] OLOFSSON O. The crystal structure of Cu<sub>3</sub>P. *Acta Chem Scand* 1972;26:2777–87.

- [57] Kulesza PJ, Pieta IS, Rutkowska IA, Wadas A, Marks D, Klak K, et al. Electrocatalytic oxidation of small organic molecules in acid medium: enhancement of activity of noble metal nanoparticles and their alloys by supporting or modifying them with metal oxides. *Electrochim Acta* 2013;110:474–83.
- [58] Kresse G, Furthmüller J. Efficient iterative schemes for ab initio total-energy calculations using a plane-wave basis set. *Phys Rev B* 1996;54:11169–86.
- [59] Kresse G, Furthmüller J. Efficiency of ab-initio total energy calculations for metals and semiconductors using a plane-wave basis set. *Comput Mater Sci* 1996;6:15–50.
- [60] Kresse G, Joubert D. From ultrasoft pseudopotentials to the projector augmented-wave method. *Phys Rev B* 1999;59:1758–75.
- [61] Perdew JP, Yue W. Accurate and simple density functional for the electronic exchange energy: generalized gradient approximation. *Phys Rev B* 1986;33:8800–2.
- [62] Luo Y-R. Comprehensive handbook of chemical bond energies. CRC press; 2007.
- [63] Aitken JA, Ganzha-Hazen V, Brock SL. Solvothermal syntheses of Cu<sub>3</sub>P via reactions of amorphous red phosphorus with a variety of copper sources. *J Solid State Chem* 2005;178:970–5.
- [64] Pfeiffer H, Tancret F, Bichat M-P, Monconduit L, Favier F, Brousse T. Air stable copper phosphide (Cu<sub>3</sub>P): a possible negative electrode material for lithium batteries. *Electrochem Commun* 2004;6:263–7.
- [65] Wells A. Structural inorganic chemistry. 5th ed. 1984. Clarendon. Oxford.
- [66] Lin C-M, Sheu H-S, Tsai M-H, Wu B-R, Jian S-R. High pressure induced phase transition in sulfur doped indium phosphide: an angular-dispersive X-ray diffraction and Raman study. *Solid State Commun* 2009;149:136–41.
- [67] Teng Y, Wang A, Li X, Xie J, Wang Y, Hu Y. Preparation of high-performance MoP hydrodesulfurization catalysts via a sulfidation–reduction procedure. *J Catal* 2009;266:369–79.
- [68] Ma L, Shen X, Zhou H, Zhu J, Xi C, Ji Z, et al. Synthesis of Cu<sub>3</sub>P nanocubes and their excellent electrocatalytic efficiency for the hydrogen evolution reaction in acidic solution. *RSC Adv* 2016;6:9672–7.
- [69] Pfeiffer H, Tancret F, Brousse T. Synthesis, characterization and electrochemical properties of copper phosphide (Cu<sub>3</sub>P) thick films prepared by solid-state reaction at low temperature: a probable anode for lithium ion batteries. *Electrochim Acta* 2005;50:4763–70.
- [70] Wagner C. Chemical shifts of Auger lines, and the Auger parameter. *Faraday Discuss Chem Soc* 1975;60:291–300.
- [71] Abu II, Smith KJ. The effect of cobalt addition to bulk MoP and Ni<sub>2</sub>P catalysts for the hydrodesulfurization of 4,6-dimethylbenzothiophene. *J Catal* 2006;241:356–66.
- [72] Han C, Pelaez M, Likodimos V, Kontos AG, Falaras P, O'Shea K, et al. Innovative visible light-activated sulfur doped TiO<sub>2</sub> films for water treatment. *Appl Catal B Environ* 2011;107:77–87.
- [73] Li Y, Zhang Y, Zhu X, Wang Z, Lü Z, Huang X, et al. Performance and sulfur poisoning of Ni/CeO<sub>2</sub> impregnated La<sub>0.75</sub>Sr<sub>0.25</sub>Cr<sub>0.5</sub>Mn<sub>0.5</sub>O<sub>3-δ</sub> anode in solid oxide fuel cells. *J Power Sources* 2015;285:354–9.
- [74] Wilson AD, Newell RH, McNevin MJ, Muckerman JT, Rakowski DuBois M, DuBois DL. Hydrogen oxidation and production using nickel-based molecular catalysts with positioned proton relays. *J Am Chem Soc* 2006;128:358–66.
- [75] Wilson AD, Shoemaker RK, Miedaner A, Muckerman JT, DuBois DL, DuBois MR. Nature of hydrogen interactions with Ni(II) complexes containing cyclic phosphine ligands with pendant nitrogen bases. *Proc Natl Acad Sci Unit States Am* 2007;104:6951–6.
- [76] Nicolet Y, de Lacey AL, Vernède X, Fernandez VM, Hatchikian EC, Fontecilla-Camps JC. Crystallographic and FTIR spectroscopic evidence of changes in Fe coordination upon reduction of the active site of the Fe-Only hydrogenase from *Desulfovibrio desulfuricans*. *J Am Chem Soc* 2001;123:1596–601.
- [77] Patel PP, Hanumantha PJ, Datta MK, Velikokhatnyi OI, Hong D, Poston JA, et al. Cobalt based nanostructured alloys: versatile high performance robust hydrogen evolution reaction electro-catalysts for electrolytic and photo-electrochemical water splitting. *Int J Hydrogen Energy* 2017;42:17049–62.
- [78] Gao M-R, Lin Z-Y, Zhuang T-T, Jiang J, Xu Y-F, Zheng Y-R, et al. Mixed-solution synthesis of sea urchin-like NiSe nanofiber assemblies as economical Pt-free catalysts for electrochemical H<sub>2</sub> production. *J Mater Chem* 2012;22:13662–8.
- [79] Shi Z, Wang Y, Lin H, Zhang H, Shen M, Xie S, et al. Porous nanoMoC@ graphite shell derived from a MOFs-directed strategy: an efficient electrocatalyst for the hydrogen evolution reaction. *J Mater Chem* 2016;4:6006–13.
- [80] Li J-S, Wang Y, Liu C-H, Li S-L, Wang Y-G, Dong L-Z, et al. Coupled molybdenum carbide and reduced graphene oxide electrocatalysts for efficient hydrogen evolution. *Nat Commun* 2016;7.
- [81] Yan H, Tian C, Wang L, Wu A, Meng M, Zhao L, et al. Phosphorus-modified tungsten nitride/reduced graphene oxide as a high-performance, non-noble-metal electrocatalyst for the hydrogen evolution reaction. *Angew Chem* 2015;127:6423–7.
- [82] Xu G-R, Hui J-J, Huang T, Chen Y, Lee J-M. Platinum nanocuboids supported on reduced graphene oxide as efficient electrocatalyst for the hydrogen evolution reaction. *J Power Sources* 2015;285:393–9.
- [83] Tang YJ, Gao MR, Liu CH, Li SL, Jiang HL, Lan YQ, et al. Porous molybdenum-based hybrid catalysts for highly efficient hydrogen evolution. *Angew Chem Int Ed* 2015;54:12928–32.
- [84] Vigil JA, Lambert TN. Nanostructured cobalt phosphide-based films as bifunctional electrocatalysts for overall water splitting. *RSC Adv* 2015;5:105814–9.
- [85] Chen Z, Jaramillo TF, Deutsch TG, Kleiman-Shwarsstein A, Forman AJ, Gaillard N, et al. Accelerating materials development for photoelectrochemical hydrogen production: standards for methods, definitions, and reporting protocols. *J Mater Res* 2010;25:3–16.
- [86] Bolton JR. Solar photoproduction of hydrogen: a review. *Sol Energy* 1996;57:37–50.
- [87] Liao C-H, Huang C-W, Wu J. Hydrogen production from semiconductor-based photocatalysis via water splitting. *Catalysts* 2012;2:490–516.
- [88] Coridan RH, Nielander AC, Francis SA, McDowell MT, Dix V, Chatman SM, et al. Methods for comparing the performance of energy-conversion systems for use in solar fuels and solar electricity generation. *Energy Environ Sci* 2015;8:2886–901.
- [89] Mi Y, Wen L, Xu R, Wang Z, Cao D, Fang Y, et al. Constructing an AZO/TiO<sub>2</sub> core/shell nanocone array with uniformly dispersed Au NPs for enhancing photoelectrochemical water splitting. *Adv Energy Mater* 2016;6.
- [90] Towns J, Cockerill T, Dahan M, Foster I, Gafter K, Grimshaw A, et al. XSEDE: accelerating scientific discovery. *Comput Sci Eng* 2014;16:62–74.